Final Report
on
Combustion Enhancements in Advanced Liquid Rocket Engines

for
AFOSR Contract/Grant F49620-97-1-0224

Prepared by

Robert J. Santoro
Propulsion Engineering Research Center
and
Department of Mechanical Engineering
The Pennsylvania State University
University Park, PA 16802

Submitted to:

Air Force Office of Scientific Research
Bolling Air Force Base
Washington D.C.

May 1999

AFRL-SR-BL-TR-99-

1999

REPORT DOCUMENTATION PAGE

0177

1. AGENCY USE ONLY (Leave blank)	2. REPORT DATE	3. REPORT TYPE AND DATES COVERED
	17 May 1999	Final Technical Report 1 Dec. 1997 - 30 Nov. 1998

4. TITLE AND SUBTITLE
Combustion Enhancements in Advanced Liquid Rocket Engines

5. FUNDING NUMBERS
PE-61102F
PR-2308
SA-AS
G-F49620-97-1-0224

6. AUTHOR(S)
Robert J. Santoro

7. PERFORMING ORGANIZATION NAME(S) AND ADDRESS(ES)
The Pennsylvania State University
240 Research Building East
University Park, PA 16802

8. PERFORMING ORGANIZATION REPORT NUMBER

9. SPONSORING / MONITORING AGENCY NAME(S) AND ADDRESS(ES)
AFOSR/NA
801 North Randolph Road, Room 732
Arlington, VA 22203-1977

10. SPONSORING / MONITORING AGENCY REPORT NUMBER

11. SUPPLEMENTARY NOTES

12a. DISTRIBUTION / AVAILABILITY STATEMENT
Approved for public release; distribution is unlimited

12b. DISTRIBUTION CODE

13. ABSTRACT *(Maximum 200 Words)*
A series of liquid jet experiments, utilizing water as the working fluid and an optically accessible orifice with a L/D ratio of 2.5, were performed using laser velocimetry to map the velocity profile at several locations within the orifice. Additional measurements were also made downstream of the orifice exit in the free jet. Finally, measurements were made for a 30° angled orifice to more closely simulate actual injector conditions. The key objective in pursuing these measurements was to determine if a correlation existed between the turbulent structures within the jet and the formation of impact waves after impingement. A link between these waves, which may play a role in combustion instability, and the boundary layer characteristics could then be used to suggest remedies for combustion instability through boundary layer modification. Velocity profile comparisons revealed no alternation of the boundary layer or turbulence characteristics. Preliminary measurements were also made in the free jet, just prior to the point of impingement. Comparison of these results revealed a significant difference between the velocity profiles and the axial turbulence intensity profiles. In particular, the impingement widens the jet and increases the turbulence found in the flow field. However, the earlier measurements indicate these disturbances did not propagate upstream to the orifice. Thus, based on this work, boundary layer thickness and turbulence effects produced in the orifice were eliminated as a mechanism for generating combustion instability in rocket combustors using impinging jet injectors. Consequentially, boundary layer modification does not appear to represent an effective approach to suppress combustion instability for these injectors.

14. SUBJECT TERMS	15. NUMBER OF PAGES
Combustion Instability, Impinging Jets, Rocket Engines, Combustion, Atomization	43
	16. PRICE CODE

17. SECURITY CLASSIFICATION OF REPORT	18. SECURITY CLASSIFICATION OF THIS PAGE	19. SECURITY CLASSIFICATION OF ABSTRACT	20. LIMITATION OF ABSTRACT
UNCLASSIFIED	UNCLASSIFIED	UNCLASSIFIED	UL

TABLE OF CONTENTS

1.0	INTRODUCTION.....	3
2.0	EXPERIMENTAL APPROACH.....	8
3.0	RESULTS AND DISCUSSION.....	20
4.0	SUMMARY.....	32
5.0	REFERENCES.....	33
6.0	PUBLICATIONS/THESES.....	34
7.0	PARTICIPATING PROFESSIONALS.....	34
	APPENDIX.....	35

1.0 INTRODUCTION

Chemical rocket technology is being driven by increasingly stringent requirements for operability, performance, and cost. The call for these requirements mandates that new or improved technologies be developed in a number of areas. Some of the new areas in which combustion is an important factor are advanced propellants, microthrusters, smart engines, and innovative rocket cycles.

Since the *injector* of the combustor provides more leverage in terms of its impact on cost and performance than any other component in the combustor, the work reported here is specifically geared towards injector-related phenomena. Research under AFOSR support in the past [Anderson et al., 1992, 1995; Anderson and Santoro, 1996; Ryan et al., 1995] has been oriented to provide a detailed description of the physical processes that cause combustion instability. The past research has been successful in providing guidance in defining some potential practical designs that should be resistant to combustion instability, such as mixing injector element types in a deliberate fashion, increasing the degree of polydispersion of the spray drop size distribution, or increasing the atomization frequency to the point where it becomes essentially continuous compared to the frequency of chamber pressure oscillations.

Based on the previous experimental and analytical results, a general hypothesis on the mechanism of combustion instability for impinging injectors was developed. According to the results, the tendency toward instability is controlled primarily by atomization. More specifically, the results indicated that the actual drop size distribution and the unsteady nature of atomization are the two most important factors that can induce combustion instability.

The AFOSR-sponsored previous research also identified the following key areas where similar benchmark quality research was necessary to significantly advance future technology within the framework of increased requirements: injector flow turbulence effects on atomization and geometric effects on flow turbulence. These areas in essence formed the roadmap for the current goal of establishing the basic science needed to provide a practical design methodology for high performance, low cost, operational injector designs which inherently possess positive combustion stability attributes. The work reported here represents the first step in completing that roadmap with the objective of providing a validated, engineering science-based design methodology for stable, high-performing injectors.

The current studies emphasize impinging jet injectors. By building on past work, the present work focuses on key injector flowfield phenomena. The studies reported here specifically address the role of turbulence and injector geometry on the atomization mechanism which, in turn, governs the stability characteristics of these injectors. Furthermore, in recognizing that injector passage geometry is a key in establishing the turbulent flow characteristics, which later are manifested in periodic atomization, the scientific basis is established for developing passive approaches to maintaining high performance and stability capabilities.

The research reported here is based on previous research under AFOSR support that showed that impact waves formed at the impingement point are highly sensitive to the nature of the jet flow. The goal of the current research was to improve understanding of the source of the impact waves in terms of basic physical phenomena. Since the detailed flow structure of the turbulent jet prior to impingement provides the key information for resolving this question, the current research is focused on providing data on the turbulence intensity spectra of liquid jets under practical atomization conditions.

During the manufacturing process of impinging jet injectors, a sharp corner occurs at the entrance to the injector orifice. As a result, the flow detaches from the orifice wall and forms a vena contracta. The vena contracta may play a role in the formation of impact waves downstream at the impingement point, and the region of the vena contracta in the flow field was therefore singled out for study under the current effort. Downstream of the vena contracta, the flow may reattach to the orifice wall prior to exit. Reattachment is governed by the orifice length and the flow velocity. For typical injectors, the Reynolds number (Re) is of the order of 10^4 to 10^5, where Re is based upon mean orifice velocity and orifice diameter. Typical L/d ratios for injector orifices are between 3 and 10. The impingement process may be linked to the flow field in the orifice; if so, modifying the orifice flow characteristics may be a viable method of controlling the atomization process and thus controlling combustion instabilities.

Combustion instability in liquid propellant rockets with impinging injectors has been a topic of research for nearly 50 years. Heidmann and Humphrey [1952] used microflash photography and atomization frequency measurements to investigate the relationships between parameters such as jet velocity, impingement angle, jet diameter, and jet length on the wave frequency observed in the spray resulting from impingement. They concluded that the velocity

of the sheet formed at the impingement had the major effect on spray frequency, with sheet velocity being influenced primarily by the jet velocity but also, to a lesser extent, by the other parameters such as jet diameter and jet length prior to impingement.

Hydraulic flip, the phenomenon where flow after the vena contracta remains detached from the orifice walls, has also been suspected of contributing to combustion instability. Hydraulic flip will occur as result of cavitation in the region of the vena contracta which then extends all the way to the orifice exit plane. Ito [1971] identified a second possible pathway for hydraulic flip, where the boundary layer growth rate is limited in orifices with small L/D ratios. This suggests that modification of the boundary layer in the injector orifice may be a possible means of controlling combustion instability if the phenomenon of hydraulic flip is related to instability.

Orifice cavitation may thus have an effect on combustion instability. Ruiz [1991] and Hoehn et al. [1972] provide some useful relationships for predicting the onset of cavitation in orifices. Ruiz's technique relies on the behavior of a cavitating orifice which makes the flow resemble that observed in a compressible flow through a nozzle. Once cavitation in the orifice occurs, the discharge coefficient drops and the flow becomes "choked," i.e. a further decrease in back pressure does not increase the flow rate. The relations developed by both Hoehn et al. and Ruiz indicate that cavitation is not occurring in the orifice used for the experiments employed in the present research, which agrees with experimental observations (i.e. no bubbles in the orifice flow). Further work is in progress to verify, using flow visualization, that cavitation bubbles are not present in the flow field. In this research, cavitation was not considered as a potential cause of instability for the operating conditions investigated.

Modification of injector orifice shape presents a possible method of controlling combustion instability which would be much less expensive than more complicated solutions such as active controls or active boundary layer modification in the orifice. Hoehn et al. [1972] experimentally measured the mixing effectiveness of several orifice shapes to determine if shape modification might be an avenue for improving combustion efficiency in liquid rocket engines. Their experiment consisted of several circular and rectangular orifices and a spherical array of collecting tubes used to collect the resulting spray from jet impingement of the various injector configurations. They concluded that insignificant differences in mixing efficiencies occur when

comparing circular and rectangular orifices, and on the basis of mixing efficiency alone there is no justification for preferring non-circular orifices over circular orifices.

The characteristic frequency of the turbulent structures in the jet may be related to observed instability frequencies. Rupe [1956] performed some pioneering work in this area to develop a dynamic head probe to measure the frequency variations in a turbulent jet impinging directly on the pressure transducer. Rupe discovered a frequency spike that corresponded to the resonance frequency of the measuring apparatus, but no characteristic frequencies which might be the source of combustion instability.

Based on this short discussion of the fluid mechanics of impinging jet injectors and its relationship to combustion instability, the goal of the present was to document the injector element flowfield. Laser Doppler velocimetry was used as the primary non-intrusive diagnostic technique for the experiments. The LDV measurements used in this research presented some challenges. Durst et. al. [1995] provided some guidance on the techniques that should be used for accurate near wall velocity measurements. Their measurements were for a fully-developed turbulent pipe flow, and they recommend the following practices:

-utilization of index-matched fluid to eliminate refraction effects;

-compensation for the finite measurement volume size of the LDV system;

-compensation for noise level in the signal due to low frequency shift;

-and, confirmation of the repeatability of the experiment by performing measurements several times.

For LDV measurements, the effect of the finite measurement volume is especially important near the wall in turbulent flows, where there is a very steep velocity gradient. Since the measurement volume is finite, i.e., does not correspond to a point, the resulting mean flow velocity really represents a spatial average, and not the velocity measurement at a point. Durst et al. [1995] arrived at a mathematical technique to eliminate this effect based upon the second derivative of the velocity, but this correction relied upon a smooth (i.e., fully developed turbulent flow) velocity profile, which was not the case with measurements taken near the vena contracta region in the present research. Instead, the measurement volume size was minimized by the method in which velocity profiles were taken, which will be discussed later.

Refractive index matching fluid, while attractive, was not practicable for the present study. Water does present some optical challenges due to the differing indices of refraction

between Plexiglas, water, and air. However, these difficulties were more than offset by the ease of working with water instead of an index matched fluid, which tends to be harder to handle (Durst et. al. [1995] used two diesel oils mixed together to achieve the matched index of refraction).

Several important objectives were established prior to the onset of this study. First, the most basic objective was to map out the flow field within a straight circular optically accessible orifice, with particular emphasis on the region of the vena contracta, since a link between observed instabilities and the vena contracta is suspected. Two-dimensional (2-D) LDV measurements were initially desired because this would determine if there was a second dimension of bulk fluid movement in addition to the axial bulk flow.

Additionally, LDV was used to investigate the flow characteristics downstream of the orifice exit, prior to impingement, in order to possibly develop a correlation between impingement and jet flow behavior.

Second, once the flow field had been adequately mapped using LDV, an angled plate was installed downstream to simulate a 60° impingement with another fluid stream. Once installed, velocity profile measurements were repeated to determine if downstream impingement had any effect on the velocity profiles observed within the injector orifice, suggesting that boundary layer in the orifice may be coupled with the downstream impingement process.

2.0 EXPERIMENTAL APPROACH

Experiments were conducted to investigate the nature of the flow characteristics in impinging jet injector orifices. Several optically accessible Plexiglas orifices, representative of injector orifices, were constructed to facilitate velocity measurements within the orifice using Laser Doppler velocimetry (LDV). Orifice geometries included circular, angled circular, conical, and rectangular. The orifices were of a larger scale than actual injector passages, to allow adequate spatial resolution when mapping the flow field.

The goal of the LDV work was to gain an understanding of the flow profile within the injector orifice. Water was used as the working fluid in the flow circuit, primarily due to ease of handling. Experiments were conducted first with the jet exiting to atmospheric pressure, and next with an angled plate installed downstream to simulate impingement with another jet. The objective was to determine if there were shifts in the boundary layer shape as a result of the impingement, and if boundary layer modification was then a possible method to remedy combustion instability problems.

The experimental flow setup is shown in Fig. 2.1. The pump used is a 20 GPM/150 psi centrifugal model. The pressure relief valve is a manual valve used to allow lower flow rates through the orifice without excessive pressure build up at the pump discharge. Cooling is

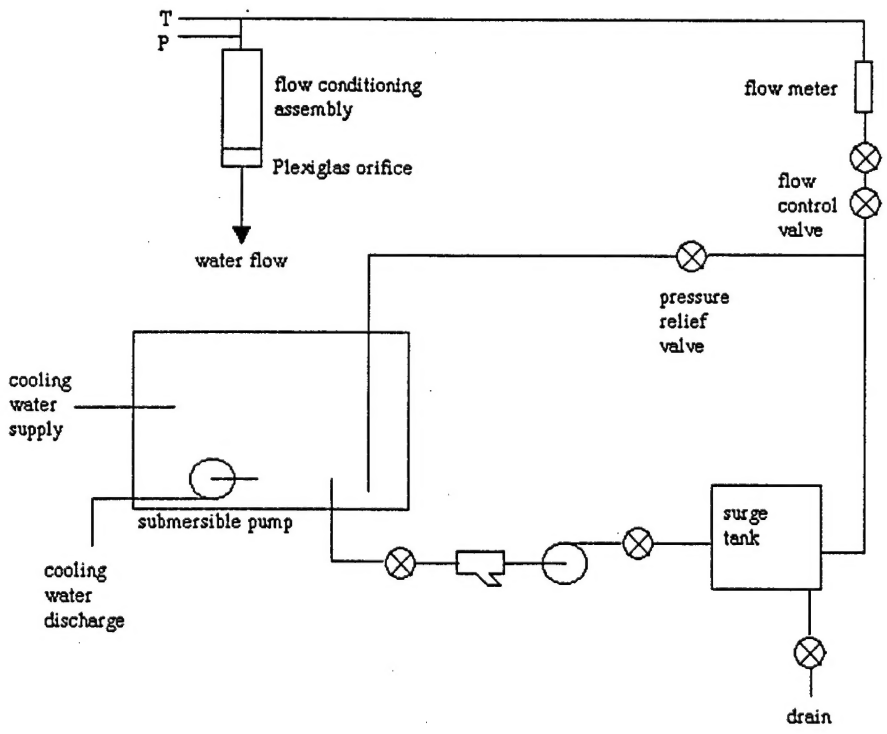

Fig. 2.1. Experimental Flow Circuit.

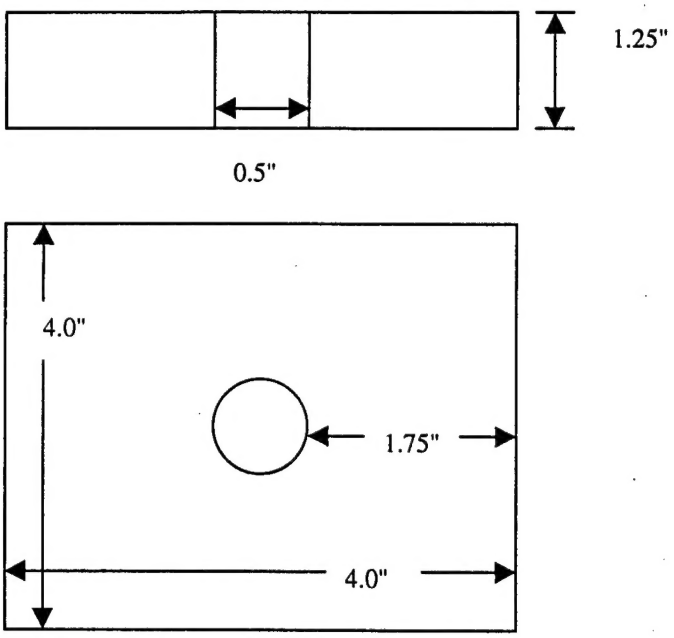

Fig. 2.2. Plexiglas Orifice.

provided by the circuit shown on the water tank, which consists of a submersible pump to remove water and a hose that provides a continuous supply of fresh, cool water. Cooling is necessary to maintain a constant temperature (and thus a constant Reynolds number). The continuous removal and replacement of the water required that seeding material, if used, had to be added continuously throughout the data acquisition process.

The flow conditioning assembly shown as part of the overall system in Fig. 2.1 was designed to provide straight, non-swirling flow to the orifice inlet to prevent undesired biasing of experimental results. This was accomplished by the use of straws in the assembly, which serve as flow straighteners, along with inlet and outlet screen assemblies.

The Plexiglas orifice is shown in Fig. 2.2. The angled orifice is similar, with the hole drilled at a 30° angle to the surface instead of the perpendicular arrangement depicted in Fig. 2.2.

This entire assembly was mounted on a milling table, which was moved to take measurements at various locations within the orifice. Moving the assembly was much simpler than providing a mechanism to move the transmitting and receiving optics in synchronism. All motion was controlled by manual adjustment of milling machine dials. Backlash in these devices mandated that profiles be taken by moving in one direction across the orifice, from centerline to wall or wall to centerline. Backtracking in the middle of a profile was avoided due to the uncertainty this generates in determining the actual position of the measurement location.

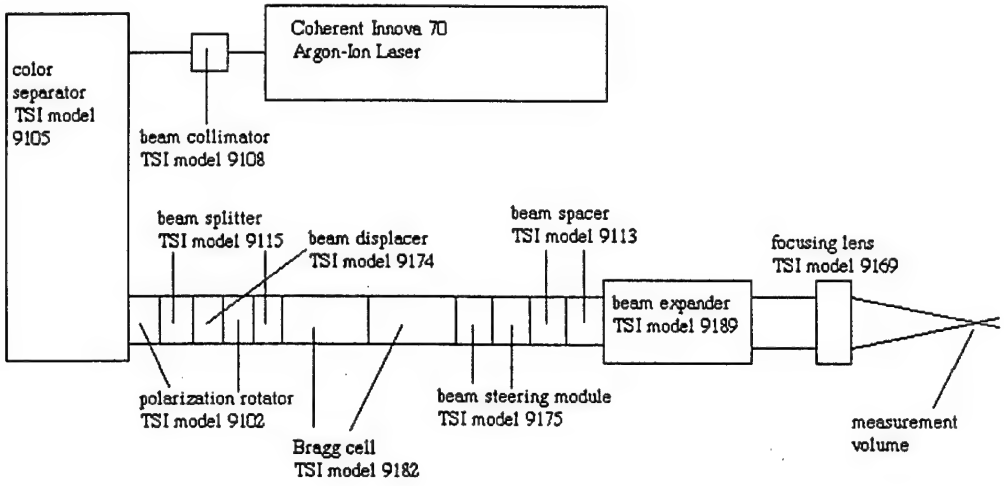

Fig. 2.3. LDV Transmitting Optics, TSI model 9100-7 2-D System.

The LDV transmitting and receiving optics are shown in Figs. 2.3 and 2.4, respectively. The other major components of the LDV system include the TSI model 9180 frequency shift system (which includes the Bragg cells shown in Fig. 2.3 and the electronics module shown in Fig. 2.4), TSI model 1990 counter-type signal processors, and a desktop computer.

An argon ion laser was used to provide the laser light, which was divided by a color separator, TSI model 9105, into a blue beam at 488 nm and a green beam at 514.5 nm wavelength. A beam splitter, TSI model 9115, was then used to split each color into two beams,

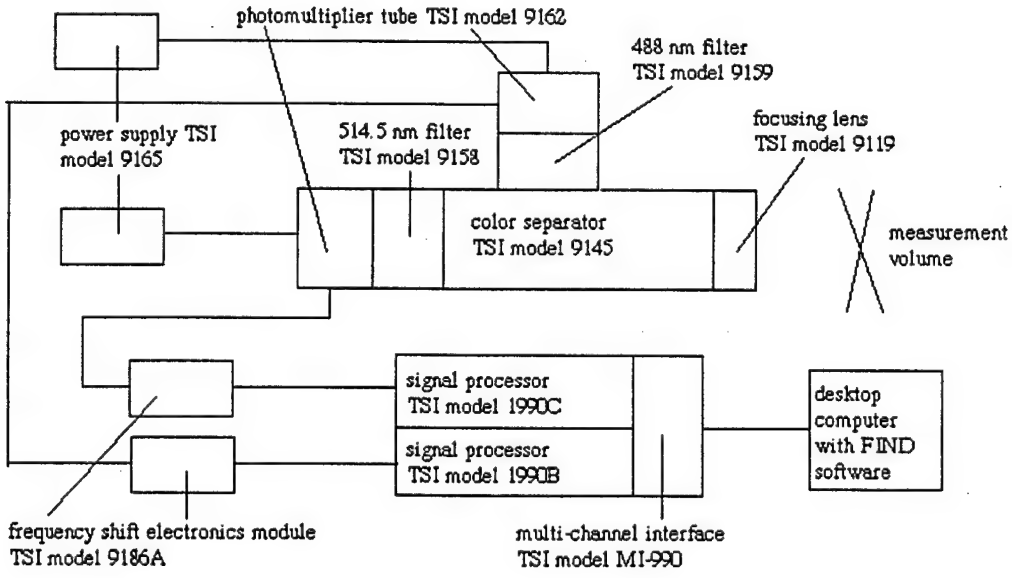

Fig. 2.4. LDV Receiving Optics and Signal Processing System.

one of which was passed through a Bragg cell, TSI model 9182. A Bragg cell was used to allow frequency shifting of one of the beams, which increased the versatility of the entire LDV system.

LDV utilizes the Doppler shift of light scattered by moving particles in the flow to determine velocity. When establishing the initial setup, the two most important concerns are ensuring that the crossing points of the beam pairs overlap (for multi-dimensional systems) and ensuring that the minimum beam diameter, i.e., the beam waist, occurs at the crossing point. Some drawbacks of the system in use here with regard to these concerns are discussed later.

An LDV system uses the relationship between Doppler shift and particle velocity to calculate the instantaneous velocity of a particle passing through the measuring volume. Since the theory of operation for an LDV system is well known, only current experiment specific information is provided here.

For the two-component experimental configuration used here, the set of green beams (514.5 nm) are used to measure the axial flow, whereas the set of blue beams (488 nm) are used to measure either the swirl or radial velocity, depending on the used optical configuration. Due to the care taken to ensure non-swirling flow into the orifice, the flow was expected to be axisymmetric with bulk flow in the axial direction only.

The dual beam system employed here is commonly used in LDV applications. It is generally preferred because it has several distinct advantages: it is the easiest to align; with one particle in the measurement volume at a time, large collection apertures can be used without violating coherence requirements; and the Doppler frequency obtained by the collecting optics is not affected by the location of the collecting optics.

The measurement volume for a dual beam measurement technique is illustrated in Fig. 2.5. The resulting measurement (or probe) volume is an ellipsoid, with the edges defined by the point where the Doppler signal drops to e^{-2} of the centerline value. For the system used in this research, the characteristics of the measurement volume are provided in Table 2.1.

The result of the narrow crossing angle used is a long, slender measurement volume, which presents some difficulties in terms of spatial resolution. When attempting to resolve the boundary layer, a probe size on the order of millimeters is clearly inadequate. Two methods were used to address and limit the effects of this problem. First, earlier work and some of the initial profiles taken during this research moved the orifice along the axis of the transmitting optics while taking velocity profiles. This was done because it presents the least optical

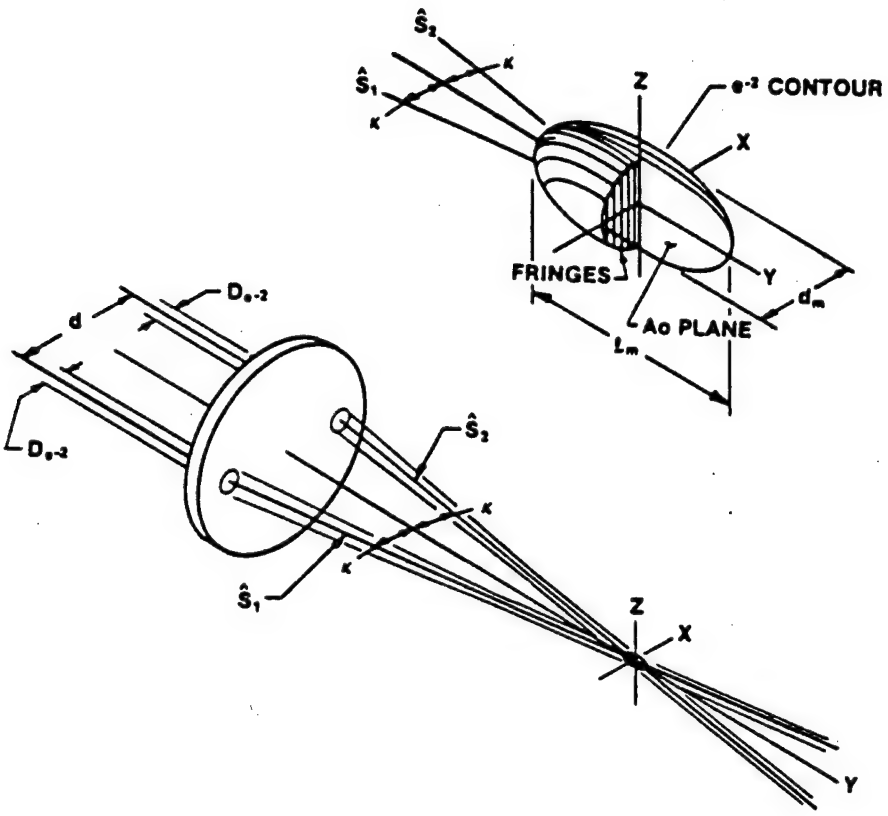

Fig. 2.5. Measurement Volume for a Dual Beam LDV System [TSI LDV Manual, 1987].

difficulty in terms of the differing indices of refraction between the three media concerned (air, Plexiglas, and water). If the orifice is maintained horizontally centered perpendicular to the axis of the transmitting optics, the green beams (which are stacked vertically) are not subject to any lensing effect by the circular walls of the orifice. Unfortunately, this means that the spatial resolution provided by the transmitting optics is on the order of the measurement volume length, which is extremely poor. This results in only 8 discrete measuring locations (no measurement volume overlap) from the orifice wall to the orifice centerline. As a result, the technique used for taking velocity profiles was changed such that the orifice was moved perpendicular to the plane of the transmitting optics, which changes the relevant spatial dimension from the measurement volume length to measurement volume diameter, an improvement of two orders of magnitude. This technique necessitated some optical corrections to locate the measurement volume correctly, as the lensing of the orifice wall bends the beams away from the centerline as the measurement volume is moved toward the wall.

To develop the required optical corrections, the differing indices of refraction, listed in Table 2.2, and the lensing effect of the circular orifice shape were considered. The corrections

Table 2.1. Characteristics of the Measurement Volume.

Characteristic	514.5 nm (green) beam	488 nm (blue) beam
Beam Waist Diameter, D_e^{-2}	5.63 mm	5.48 mm
Probe Volume Diameter, d_m	88.8 μm	84.2 μm
Probe Volume Length, l_m	1.64 mm	1.55 mm
Fringe Spacing, d_f	4.77 μm	4.41 μm
Number of Fringes, N_{FR}	18.6	19.1

that follow were developed for the green measurement volume only. These values were determined using published material properties, with the recognition that the actual values observed might be slightly different.

The location of the measurement volume was calculated using the indices of refraction given above, and this was compared to the observed locations of the centerline and the wall (based on visual observation, velocity values, and data rate). The values were close, as expected, but not in perfect agreement. Adjusting the index of refraction of the Plexiglas to 1.441 in the calculations allowed the calculated and experimental values to agree. The calculated measurement volume location is shown in Fig. 2.6.

These calculations were validated by measuring the index of refraction of the water. This was accomplished by measuring the optical distance across the orifice while moving parallel to the axis of the transmitting optics. The distance the orifice must be translated to move the measurement volume from one wall to the other is a function only of the index of refraction of the water, and is unaffected by the refractive properties of the Plexiglas. While simple in concept, this technique is complicated by the large length of the measurement volume for the beams, which renders determining when the measurement volume meets the wall nearly impossible to do with a great deal of accuracy. Thus this measurement was not a precise

Table 2.2. Indices of Refraction Used for Optical Corrections.

Medium	Index of Refraction (n_{medium})
air	1.0
water	1.33
Plexiglas	1.5

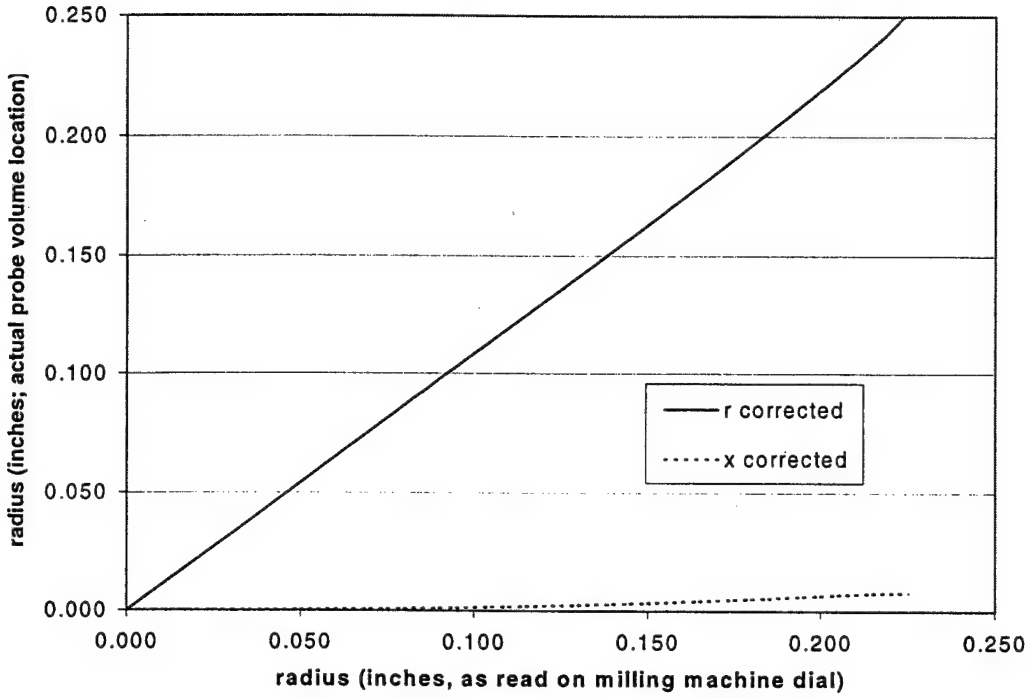

Fig. 2.6. Movement of Green Beam Measurement Volume.

calculation, but was used as a check to see if the value of index of refraction for water was reasonable. This measurement did provide reasonable agreement with the tabulated value of 1.33 used for the index of refraction of water.

In Fig. 2.6, r corrected represents the movement of the measurement volume parallel to the scan direction; x corrected represents the movement perpendicular to the scan direction. As shown, the movement parallel to the scan direction (in line with the receiving optics) is linear, so this is a relatively simple correction. The movement perpendicular to the scan direction is minimal compared to the length of the measurement volume (measurement volume length is approximately 0.065 inches) and this effect was neglected when taking measurements. By scanning in this manner, the spatial resolution in the scan direction (based on the transmitting optics) is improved from 0.065 inches to 0.003 inches, an order of magnitude improvement.

The second method to improve the spatial resolution of the system is off-axis collection of the scatter light. The measurement volume size is affected not only by the transmitting optics, but also by the receiving optics. If the receiving optics are on the same axis as the transmitting optics, the two measurement volumes are the same; as the receiving optics are moved off axis, a separate measurement volume, based on the receiving optics only, can be developed. Therefore,

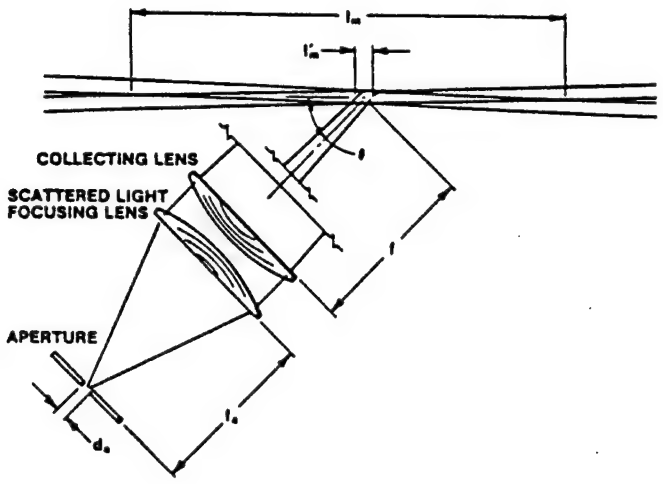

Fig. 2.7. Off-axis Collection Technique [TSI LDV Manual, 1987].

spatial resolution can be improved by moving the receiving optics off-axis and configuring their optics such that a smaller measurement volume results. This arrangement is depicted in Fig. 2.7.

The setup utilized in this research employed off-axis collection with the receiving optics mounted at a 90° angle to the transmitting optics. The receiving optics aperture, which was mounted inside the photomultiplier tube (TSI model 9160), has a diameter of 250 μm, and the resulting measurement volume length, l_m', is 750 μm. This represents a 50% reduction in measurement volume length over the measurement volume length provided by the transmitting optics.

Two issues must be quickly addressed here. First, comparison of the measurement volume lengths provided by the transmitting and receiving optics with the measurement volume movement perpendicular to the scan direction justifies neglecting the slight movement of the measurement volume in this direction as a profile is taken. The total measurement volume movement perpendicular to the profile scan direction is much less than the length of either measurement volume.

Second, off-axis collection combined with adjustments to the receiving optics configuration can yield significant reductions in measurement volume length. However, the 750 μm measurement volume length provided by the receiving optics is still inadequate to resolve the boundary layer of the flow; the measurement volume length is an order of magnitude larger than the measurement volume diameter, which is only affected by the transmitting optics configuration. No adjustment of the receiving optics can affect the measurement volume

diameter. Therefore, determination of velocity profiles by moving in line with the receiving optics (mounted 90° off-axis) allows the measurement volume diameter to be the controlling parameter in determining spatial resolution, and therefore results in the best possible spatial resolution for this system.

An additional technique for reducing measurement volume size which was implemented in the LDV system is the use of beam expansion. The equations for calculating measurement volume diameter reveal that increasing the focal distance of the transmitting lens also increases the measurement volume dimensions. Beam expansion through a negative-positive lens combination results in an increase in beam spacing and beam diameter; however, since both increase equally, the number of fringes is unchanged. The resulting increase in beam diameter causes a decrease in both measurement volume diameter and length, improving spatial resolution. The beam expander, TSI Model 9189, provided an expansion ratio of 3.75.

Increased spatial resolution could be achieved by decreasing the diameter of the measurement volume. The approach of off-axis collection can be used to reduce measurement volume length, but this technique has no effect on measurement volume diameter. In fact, a minimum measurement volume diameter can be defined that is dependent on the capabilities and settings of the signal processor, not the optics.

The issue here is not the optical setup but the measuring limitations of the signal processing equipment. The signal processing equipment provides the absolute limit on the resolution capability of the LDV system. It should be noted that while this method appears to provide a reduction in measurement volume size (and thus an improvement in spatial resolution) without any modification of the optics, this is not actually the case. While the measurement location is actually smaller than the optically defined measurement volume, there is no method available to ascertain exactly where within the measurement volume the measurement occurred. Thus, the measurement volume defined by the signal processing equipment should be thought of as a lower limit on spatial resolution, and not as a way of improving resolution without optical modifications.

In previous work, 1 μm Al_2O_3 particles were used to seed the flow. When making measurements for the current research, use of these particles did not provide increased data rate and actually lowered the data rate in some instances. Alternative seeding particles were investigated, and milk proved to be the best seed, usually causing a three to fivefold increase in

data rate. For all measurements, milk was added either 20 ml at a time (to a water volume of approximately 20 gallons) to maintain a constant level of seeding, or via a continuous drip. In either case, seed level was adjusted to maximize data rate. Adding too much milk actually lowered the data rate, so in all cases the seed level was kept slightly below this value.

Frequency shifting was accomplished using a Bragg cell, as part of the TSI model 9180 frequency shift system. Frequency shifting allows the measurement of the direction of the velocity components and is therefore essential in the 2-D setup. In the absence of frequency shifting, LDV only determines the magnitude of the velocity component. The green beams were used to provide measurement of the flow velocity in the axial direction, while the blue beams provided the ability to measure flow in either the angular or radial direction within the circular orifice. Frequency shifting for the determination of flow direction was not so critical for the green beam measurements, but critical to any use of the data provided by the blue beams. Frequency shifting was also employed in this experiment because it allows the optimization of the measurement frequency, and thus maximization of the data rate.

The receiving optics assembly consisted of a color separator (TSI model 9145), and a receiving optics assembly which separated the green and blue scattered light, respectively, and directed the light to two photomultiplier tubes (TSI model 9160) which received and amplified the light signal from the green and blue beams. The signal was then input to the frequency shifting electronics module (TSI model 9186A), which controls the shift produced by the Bragg cell, and modifies the signal to remove the shift imposed upon the laser beams themselves. This was then output to a TSI 1990C counter type signal processor (green beam signal) or a TSI model 1990B (blue beam signal) and the two signals were merged by a TSI model MI-990 interface and sent to a desktop computer for data evaluation, storage, and output.

The TSI 1990 counter allows the measurement of a predetermined number of cycles (in the LDV application, a desired number of Doppler bursts or data points) while most processors measure the number of cycles for a given time. The 1990 processor consists of a power supply, input conditioner, timer, and a readout module. The input conditioner allows the adjustment of several parameters, including high and low filtering, gain, amplitude limit, processor mode, cycles per burst, and % comparison, which must be properly adjusted to achieve proper output. For all measurements conducted here, the processor was operated in counter

mode, with the gain set near 1, and cycles per burst was maximized consistent with maintaining an acceptable data rate. Settings used for individual measurements are noted below.

TSI's Flow Information Display (FIND) software was used to evaluate and display the velocity data. The FIND software performed all of the statistical calculations necessary to generate a mean velocity, and calculate higher moments such as the turbulence intensity. The FIND software was also used to perform some spectral analysis of the velocity data, in order to determine the presence of characteristic frequencies that might be present in the flow field. Velocity averages and turbulence intensity values were also recorded and entered into spreadsheet software for plotting and graphical evaluation.

Initial experiments showed mean swirl velocities typically very near zero with large turbulence intensities (sometimes over 1000%) and no discernable trend. This data was not reproducible, and was dismissed as random fluctuations due to turbulence in the flow. 2-D work also presented the additional complication of possible non-overlap of the green and blue measurement volumes, due to the differing wavelengths of the light. It was determined that the additional efforts required to collect swirl velocity data using the 2-D system were not justified in light of the inconclusive and non-reproducible data that were provided by the blue channel, and the expectation, due to experimental setup, that no swirl velocity was present. As a result, the 2-D effort was abandoned and efforts instead focused on 1-D measurements.

The following settings are representative of those used for all measurements:

Frequency Shift: up 1 MHz

Filter Settings: high limit 5 MHz, low limit 100 kHz

Gain: approximately 1

Amplitude Limit: 1.0

Processor Mode: counter

Comparison: 1%

Cycles per Burst: 16

The frequency shift and filter limits used result in an observable velocity range of -4.0 to 18.0 m/s, which is reasonable for the velocities expected. All data was taken with the inline flow meter set to 15 GPM, which corresponds to an actual flow rate of 14.45 gallons/minute, based on a calibration table for the flow meter developed during previous work with the system. Some measurements were taken with the low frequency filter in the off position, but this did not appear

to affect the results in any way. Observation of histograms showed that the frequency limits used were reasonable.

Profiles were initially taken at the three x/D locations, and then a plate was installed approximately 2.5 inches (5 orifice diameters) downstream to ascertain if there was any observable difference in either the velocity profiles or the frequency response. The plate was angled to simulate a 60° impingement, typical of setups used in practical applications.

Other orifice geometries were considered, including conical, rectangular, and an angled circular orifice that more closely resembles the actual configuration encountered in practical impinging jet injectors. Lack of encouraging results favoring boundary layer modification as a mechanism for rectifying combustion instability resulted in a curtailing of this effort after investigations of the two circular orifices (straight and angled).

3.0 RESULTS AND DISCUSSION

LDV measurements of various simulated injector flow regimes were conducted. Initial efforts were focused on a straight cylindrical orifice designed to model a single injector orifice passage, and particularly upon the vena contracta region of the flow. Refinements in the measurement technique led to additional investigations at different locations to study the effects of downstream impingement on the orifice flow. Subsequent efforts were directed towards an angled orifice, which more realistically simulates the non-symmetric flow conditions found in an injector orifice. Finally, measurements were conducted downstream of the injector exit to study the flow profile within the jet just prior to impingement. All profiles were taken using 50,000 data points to establish mean quantities at each measurement location, unless otherwise noted.

Initial measurements were directed towards providing a picture of the development of the vena contracta in the region near the orifice inlet, since it was suspected that the effects of downstream impingement might cause a difference in vena contracta development and therefore suggest a link to combustion instability. The measurement setup is illustrated in Fig. 3.1. These initial profiles were taken by scanning along the axis of the transmitting optics, which is optically the simplest case since no optical corrections are required. The green beams, which are in the same vertical plane, are not subjected to any lensing effect by the orifice since they are always maintained on the centerline. Unfortunately, as discussed earlier, this is not the optimal approach for spatial resolution. The governing dimension is measurement volume length as determined by the receiving optics, which in this case is 750 μm, or 0.030 in., i.e. approximately

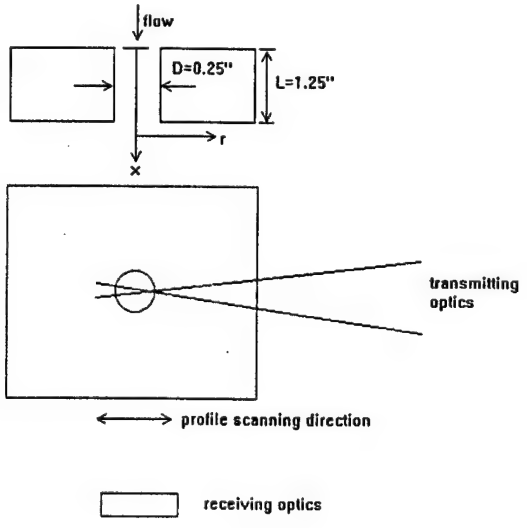

Fig. 3.1. LDV Measurement Setup in the Straight Circular Orifice.

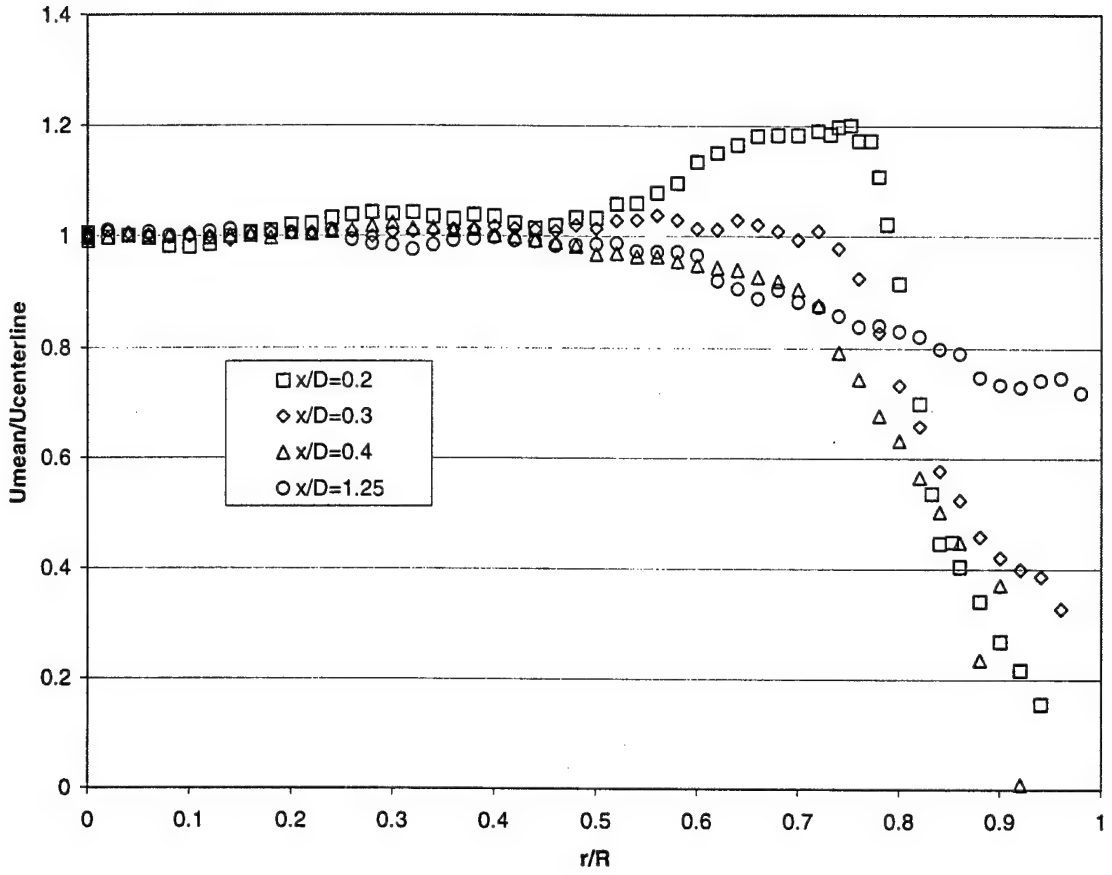

Fig. 3.2. Vena Contracta Development in the Straight Circular Orifice for Re_D=79,400

12% of the radius of the orifice itself. Spatial resolution was optimized in subsequent measurements by scanning perpendicular to the axis of the transmitting optics.

The results of the initial vena contracta measurements are shown in Fig. 3.2. These profiles are normalized in terms of the centerline velocity for each profile, and the radius of the orifice. The presence of the vena contracta at x/D=0.2 is clearly evident from the velocity profiles shown in Fig. 3.2, whereas by x/D=0.4 it has almost disappeared. The region of the vena contracta is confined to the top 1/5 of the orifice. Measurements upstream of the x/D=0.2 location were not possible due to optical inaccessibility.

These and all subsequent measurements were taken at a flow rate 14.45 gallons per minute, which for this case resulted in a flow Reynolds number, Re_D of 79,400. There was some variation in flow Re_D during the course of this research due to slight variations in water temperature, but Re_D differences are incidental and not intentional. Studying the effects of

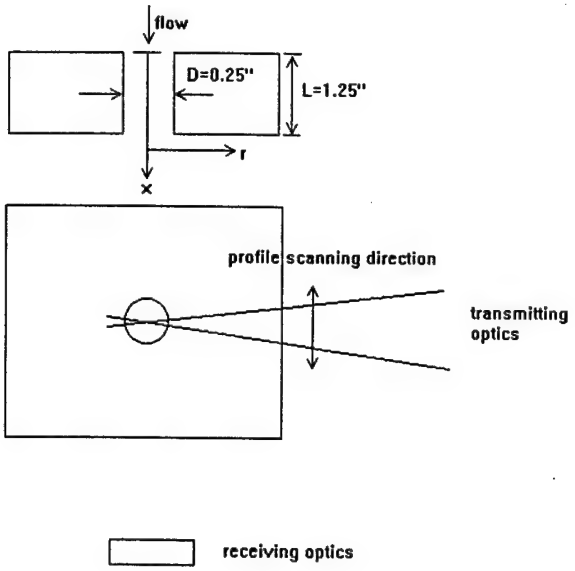

Fig. 3.3. LDV Measurement Setup in the Straight Circular Orifice.

varying Re_D on the injector flow profiles was not a goal of this research. All values of Re_D used for this investigation are referenced to the orifice diameter, D.

The vena contracta thus observed extends nearly 1/3 of the way into the orifice and causes a large "bubble" around which the flow must accelerate due the effectively smaller orifice area. After the vena contracta region, the flow reattaches to the wall and at downstream locations a typical turbulent flow profile develops.

After these initial investigations, the measurement technique was modified, as discussed earlier, to provide better spatial resolution. All subsequent velocity profiles were obtained by moving the flow assembly in the plane of the receiving optics, making the measurement volume diameter (instead of the length) the controlling parameter. This improved the spatial resolution from 750 μm (0.030 in.) to 89 μm (0.003 in.), an order of magnitude improvement. This provided for a much better picture of the boundary layer, which was necessary to determine the effects of downstream impingement on the boundary layer within the orifice. The measurement setup and scanning direction are illustrated in Fig. 3.3.

Initially, velocity profiles were taken at the extreme ends of the orifice and at the midpoint of the orifice, to establish a picture of the flow development within the orifice. The flow profiles obtained at these locations are shown in Fig. 3.4. The profiles clearly show the presence of the vena contracta at x/D=0.2, with downstream flow reattachment and boundary layer growth. These profiles are not directly comparable to those shown in Fig. 3.2 due to the

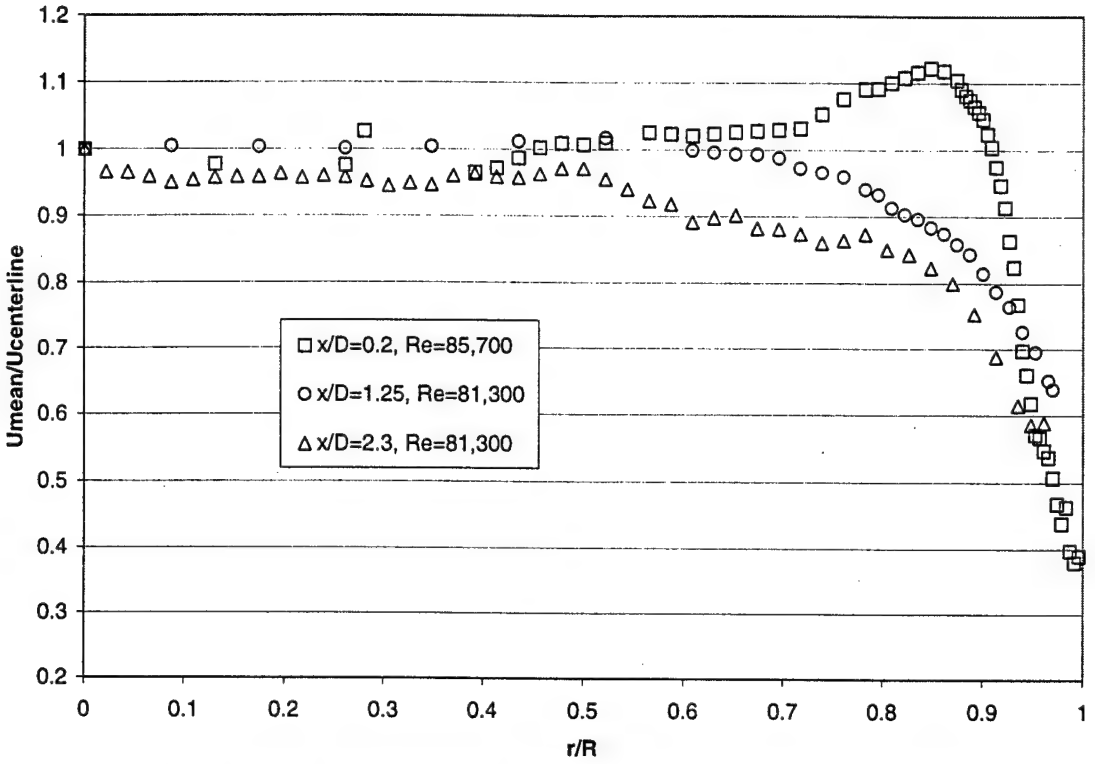

Fig. 3.4. Flow Development within the Straight Circular Orifice.

difference in measurement technique, since different scan directions were used. The profiles shown in Fig. 3.4 are more representative of the actual velocity profile due to the improved spatial resolution. Differences in Re_D are incidental (again, due to slight variations in system water temperature) and are not considered to compromise the comparability of the measurements at the different locations. This was verified by integrating the velocity profiles to determine the volumetric flow rate; the flow rate at all three locations agrees within 10% of that indicated on the installed flow meter, indicating the flow conditions were essentially the same.

Comparison of the turbulence intensity profiles at the three locations again confirms the picture shown by the velocity profiles. The axial turbulence intensity profiles are shown in Fig. 3.5, where the normalized axial turbulence intensity is defined as

$$I_x = u'/U$$

where

I_x = axial turbulence intensity

u' = standard deviation of the velocity

U = mean velocity

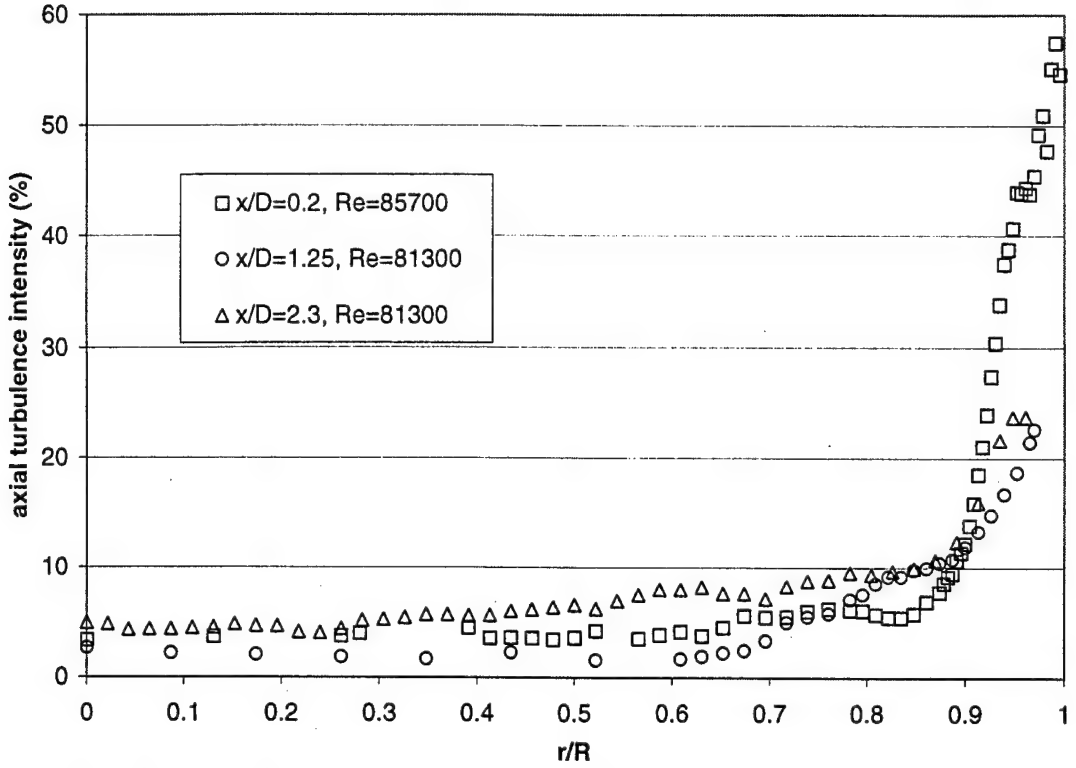

Fig. 3.5. Axial Turbulence Intensity within the Straight Circular Orifice.

Outside the boundary layer, the turbulence intensity profiles are similar at all three locations. Within the boundary layer, the x/D=1.25 and x/D=2.3 profiles are similar, but the x/D=0.2 profile reveals a much larger and more rapid increase in turbulence intensity as a consequence of the presence of the vena contracta.

Upon completion of these initial orifice measurements, an angled plate was installed downstream of the orifice exit to simulate impingement with another fluid stream. Impingement angles are typically 45° to 90°, and for these experiments the plate was angled at 30° to the jet to simulate a 60° impingement angle. The two injector elements are typically spaced to provide impingement between 3 to 10 orifice diameters downstream. The plate apparatus shown in Fig. 3.6 causes impingement 2.42 inches, or 4.84 orifice diameters downstream.

Measurements were repeated at x/D=0.2 and x/D=1.25 with the plate installed for comparison with earlier profiles to determine the effect of downstream impingement upon the orifice flow characteristics. Flow profiles with the plate removed were also repeated to verify reproducibility and ensure comparability to impinging jet profiles. The two profiles at x/D=0.2 are shown in Fig. 3.7. As Fig. 3.7 shows, there is no alteration of the boundary layer profile in

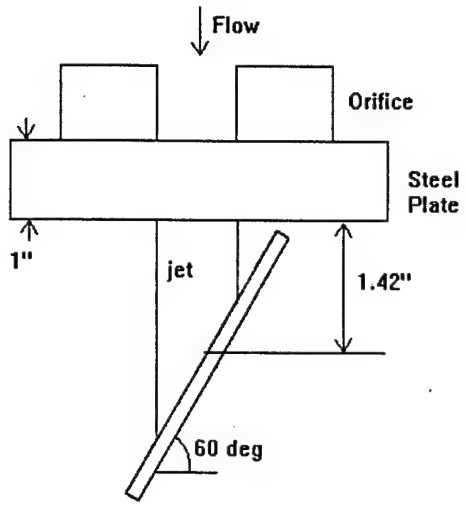

Fig. 3.6. Impingement Plate Apparatus.

the vena contracta region due to downstream impingement, which removes this effect as a possible cause of combustion instability. The slight separation of the two profiles near their peak is less than the spatial resolution capability of the LDV system and is therefore not significant.

In addition to comparing velocity profiles, power spectral density analysis of the profiles was performed using the FIND software; no alteration of the frequency content of the flow field

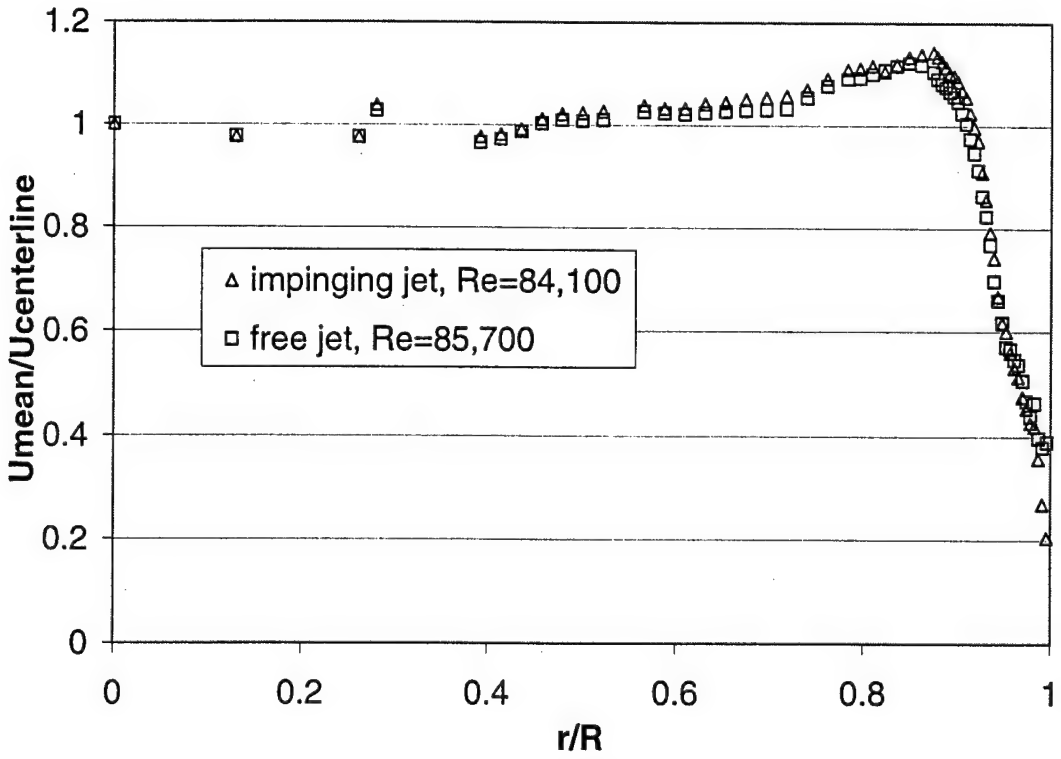

Fig. 3.7. Normalized Mean Velocity Profiles at x/D=0.2.

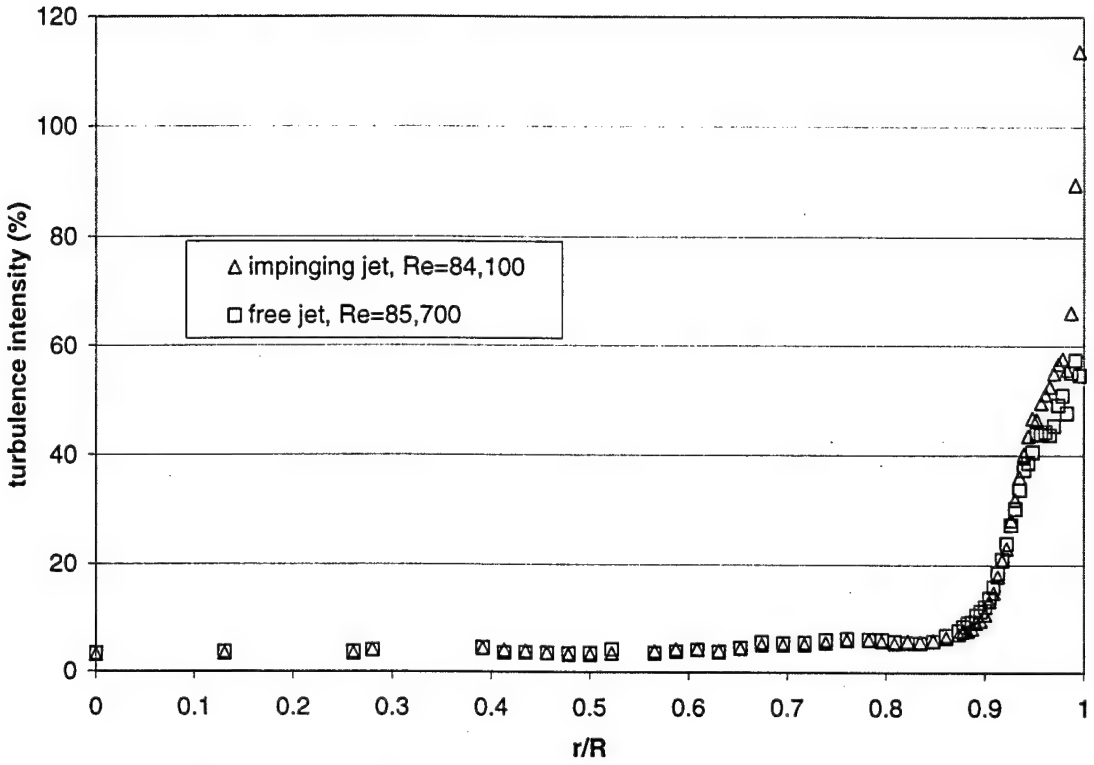

Fig. 3.8. Axial Turbulence Intensity Profiles at x/D=0.2.

was observed. Comparison of the turbulence profiles at these two locations also reveals no difference between the free jet and the impinging jet, as shown in Fig. 3.8.

Similar measurements were obtained at x/D=1.25 to confirm that there was no measurable difference between the flow profiles for the impinging and the free jets. The flow profiles are shown in Fig. 3.9. Frequency spectra were also compared as was done for the x/D=0.2 profiles, with no observed alteration of frequency content. Turbulence intensity profiles are also the same, as shown in Fig. 3.10.

These results indicate that downstream impingement does not affect the orifice flow characteristics and therefore is not a method for controlling combustion instability. To confirm this result, further investigations were pursued using an angled orifice that more closely resembles the actual, non-symmetric flow conditions found in an impinging jet injector. The angled orifice used was identical to the straight circular orifice previously used, but with the 0.5 inch diameter hole drilled at 30° to the face of the orifice, thus simulating an injector element with a total impingement angle of 60°. To allow the use of the 1-D LDV system to measure the axial velocity, the entire assembly was rotated 30° in the plane of the receiving optics such that

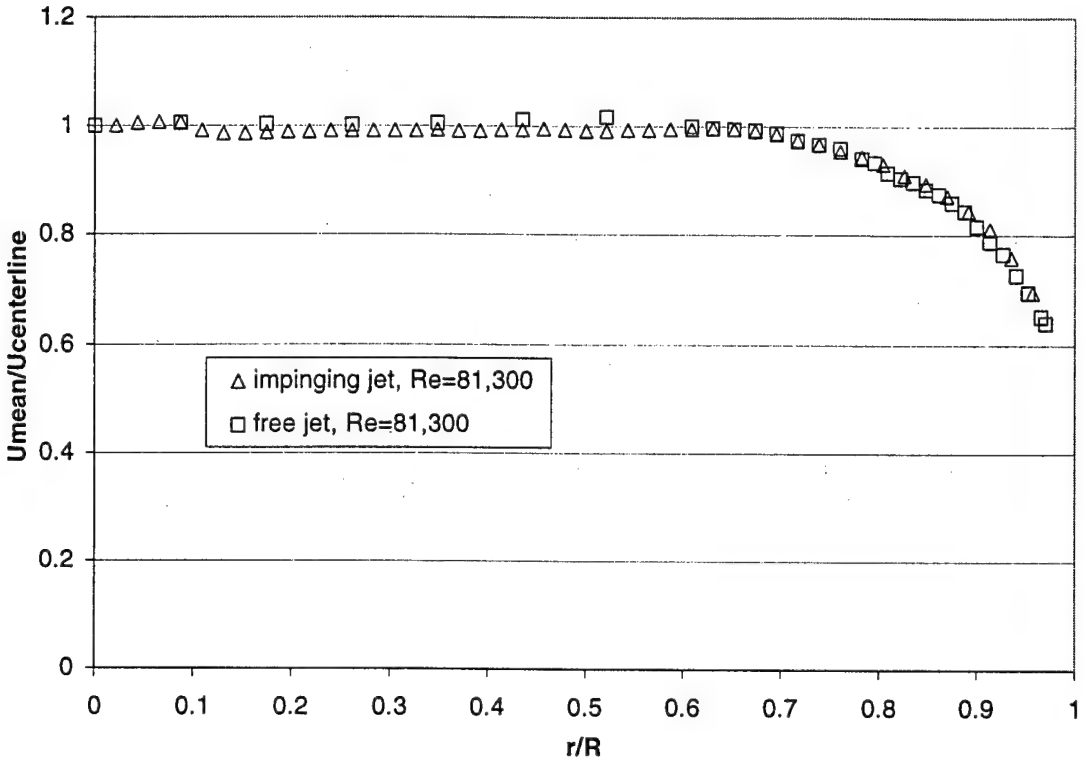

Fig. 3.9. Normalized Mean Velocity Profiles at x/D=1.25.

the circular passage was vertical. This arrangement is depicted in Fig. 3.11, along with the orientation used for profile scans. Optical accessibility was limited due to the skewed arrangement of the entire assembly, which resulted in the steel support mountings for the orifice

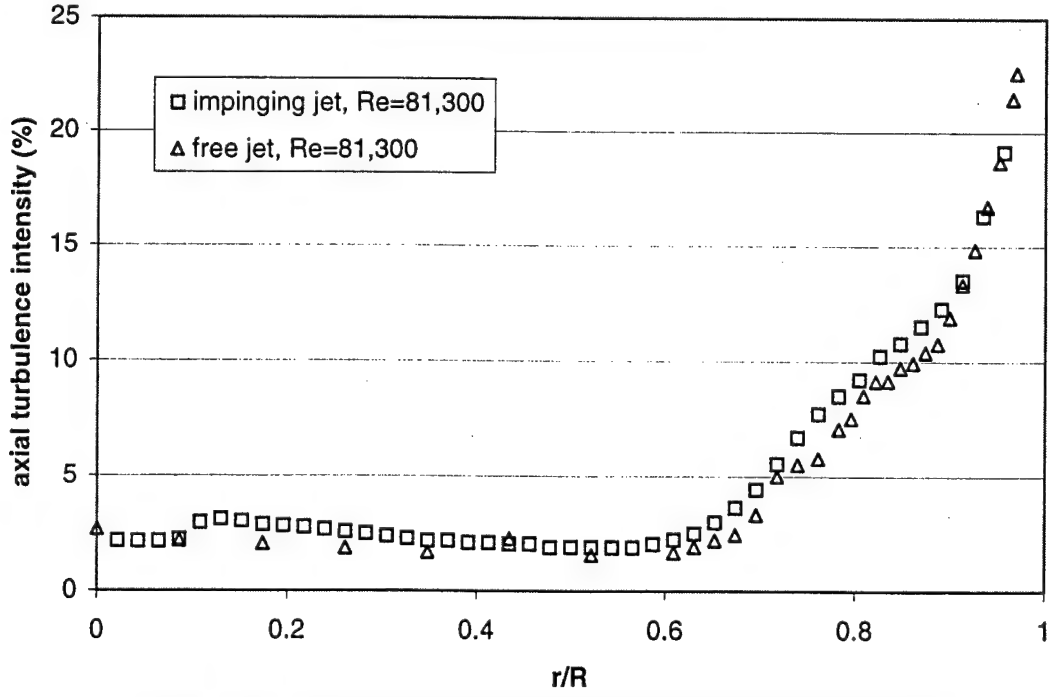

Fig. 3.10. Axial Turbulence Intensity Profiles at x/D=1.25.

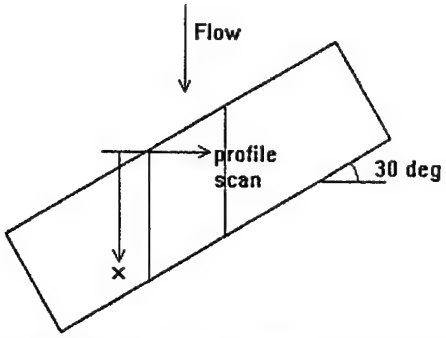

Fig. 3.11. Angled Orifice Measurement Technique and Location.

plate interfering with the receiving optics. This allowed the capturing of profiles only very near the top or bottom of the flow field, depending upon which way the angled orifice was mounted. Measurements were taken at extreme upstream and downstream locations.

The results of the angled orifice velocity measurements are shown in Fig. 3.12. Both the velocity profiles and the axial turbulence intensity profiles were compared to evaluate the presence of any disturbance in the flow due to the presence of the plate downstream. The turbulence intensity profiles are shown in Fig. 3.13. Both sets of profiles indicate that there is no measurable difference between the two flow conditions, again indicating that boundary layer modification is not a viable mechanism for controlling combustion instability.

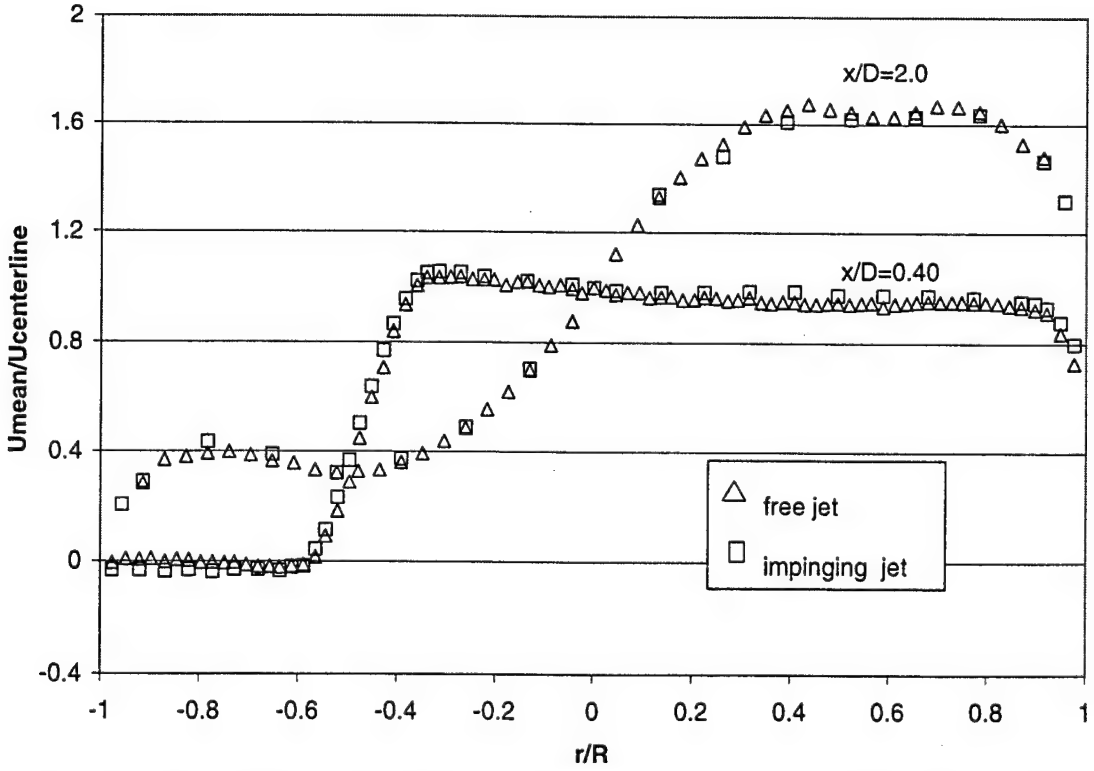

Fig. 3.12. Normalized Axial Velocity Profiles in the Angled Orifice, Re_D=90,900.

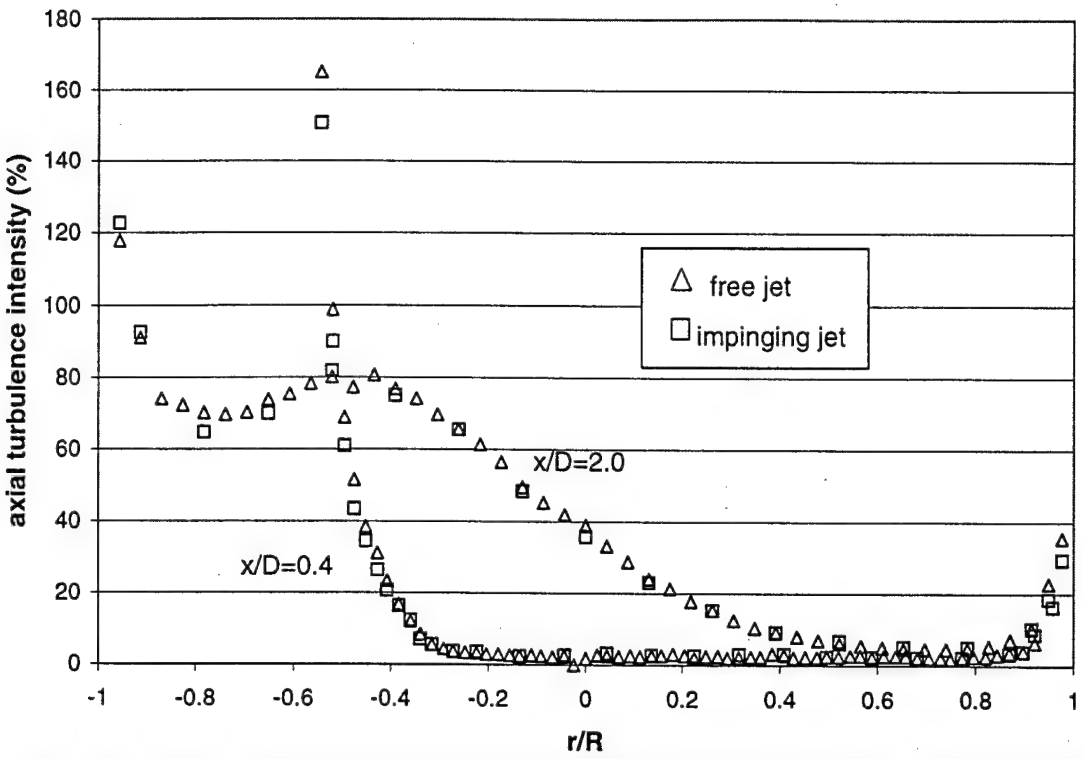

Fig. 3.13. Axial Turbulence Intensity Profiles in the Angled Orifice, Re_D=90,900.

A final measurement was made beyond the orifice in the jet itself, again both with and without downstream impingement. This measurement was made such that one side of the profile was on the angled plate surface (for the impinging case) and moved across the jet to the far boundary. Since it was closest to the point of impingement, this approach held the most promise for detecting any upstream affects of the impingement. The profiles were taken at x/D=3.65, such that the right hand side of the plot represents the point where the jet edge intersects the angled plate for the impinging jet, as shown in Fig. 3.14.

Unlike the other profiles, which are based on 50,000 data points, these profiles are based upon an average of 10,000 data points at each location, due to the significantly lower data rates experienced when conducting measurements in the jet. As such, the results depicted here should be considered preliminary.

Fig. 3.15 shows the results of this comparison measurement. The velocity is normalized by the theoretical orifice velocity (calculated using the flow rate of 14.45 gallons per minute, the orifice area, and assuming a plug flow profile). The spatial coordinate is normalized by the orifice diameter. Three profiles were taken: first, a detailed profile within the free jet, then a detailed profile with the plate apparatus installed, followed by a repeated measured profile with the plate removed to verify reproducibility.

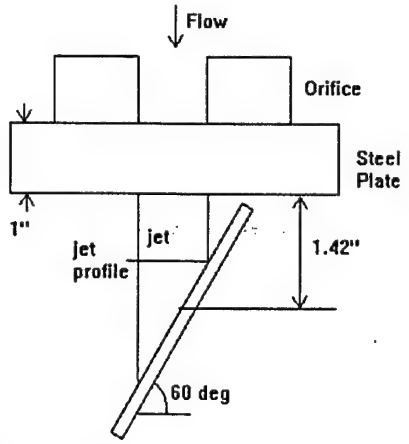

Fig. 3.14. Jet Measurement Arrangement.

There is a marked difference between the two profiles. First, while on the left side of Fig. 3.15 both jets have an air/water boundary at the same location, the impinging jet extends further to the right. This is probably due to the impingement of the jet with the plate, which creates a zone where the water is recirculated upstream as it strikes the plate. What results is similar in shape to the profile observed for the vena contracta in the orifice, with a sharp boundary layer leading to the peak velocity observed in the flow field. The lower velocity observed in the middle of the flow field may be due to the downstream impingement, but the

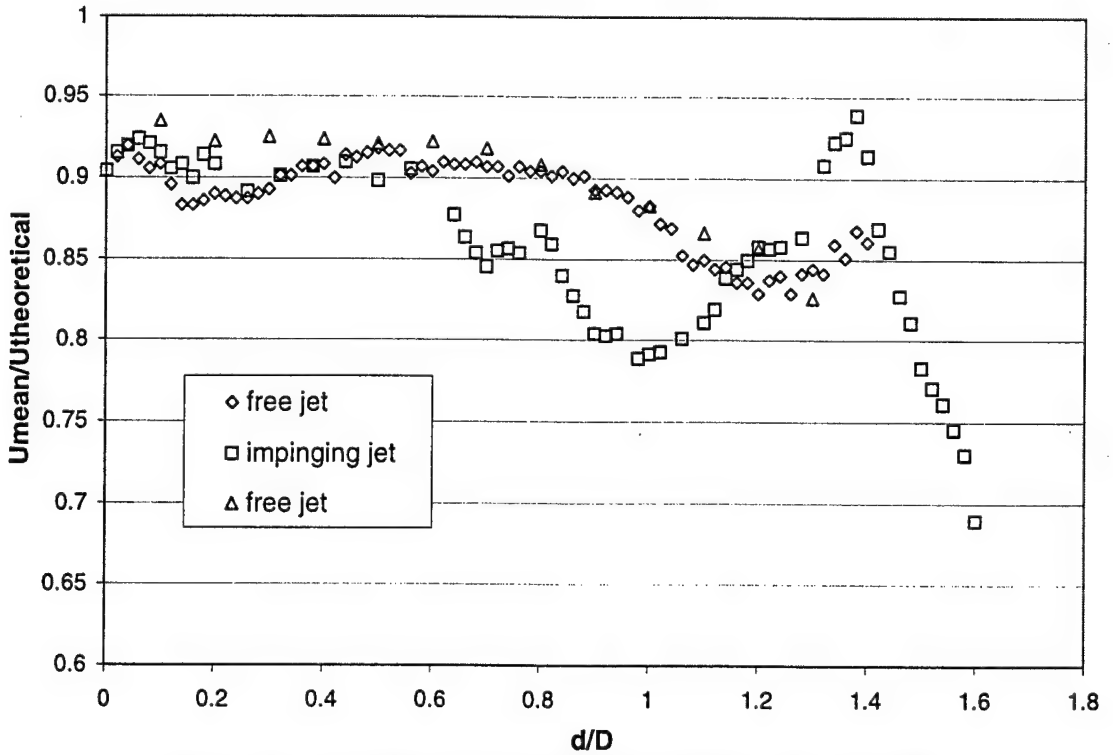

Fig. 3.15. Normalized Jet Velocity Profiles, Re_D=102,300.

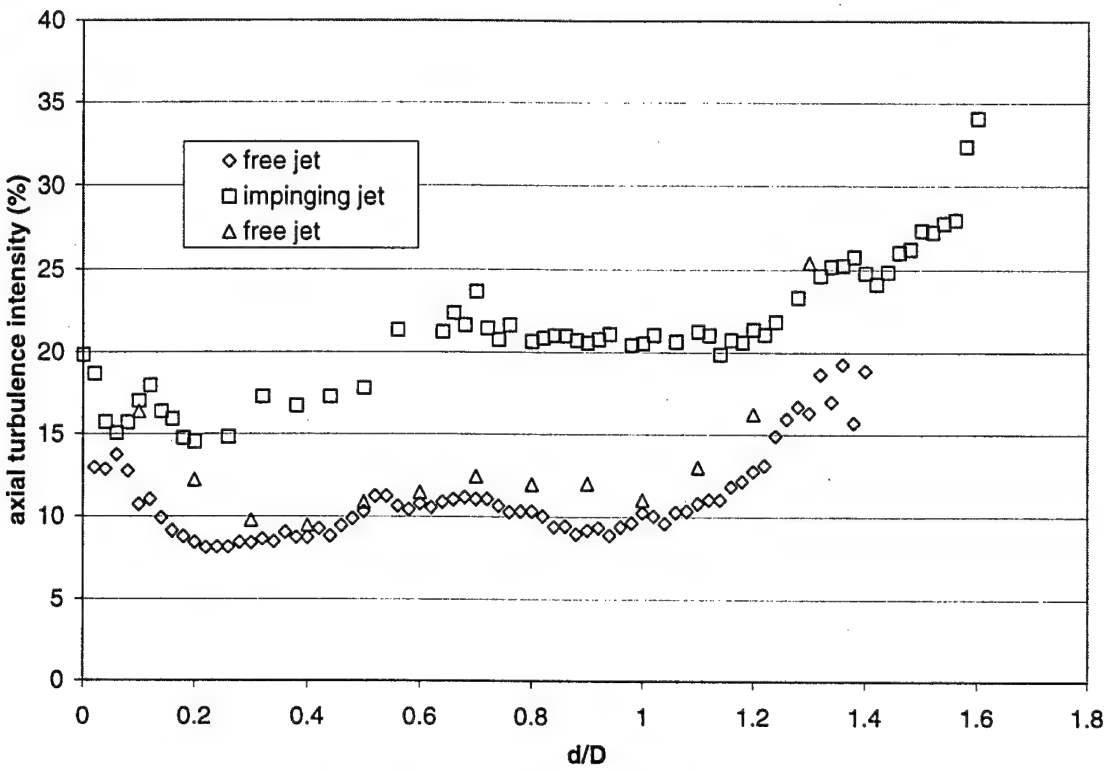

Fig. 3.16. Jet Axial Turbulence Intensity Profiles, Re_D=102,300.

origin of the peak is somewhat unclear; it may be due to upstream flow diverted and accelerating around the stagnation point where the outer edge of the jet strikes the plate. The asymmetric free jet profile is unexpected, since the experiment was carefully designed to provide axisymmetric flow through the orifice, and preliminary measurements in the straight circular orifice verified that the flow was indeed axisymmetric. The complementary turbulence intensity profiles for the same measurements are shown in Fig. 3.16.

These measurements indicate the presence of greater turbulence in the impinging jet stream, indicating that the downstream impingement does have an effect upon the flow characteristics immediately upstream of the impingement point, unlike the results observed earlier with the injector orifice itself. Thus, downstream impingement does have an effect on the turbulent flow characteristics, but these effects appear to be significant only in the immediate vicinity of the impingement. Elsewhere, the effects are not measurable. This suggests that impingement may be linked to combustion instability through alteration of the turbulent structures in the impinging jet. However, these effects are not propagated upstream into the orifice, so boundary layer modification within the orifice does not appear to be a viable method for combating combustion instability.

4.0 SUMMARY

A series of liquid jet experiments, utilizing water as the working fluid and an optically accessible orifice with L/D=2.5, have been performed using LDV to map the velocity profile at several axial locations within the orifice. Additional measurements were also made downstream of the orifice exit in the free jet. Finally, measurements were made for a 30° angled orifice to more closely simulate actual injector conditions. The key objective in pursuing these measurements was to determine if a correlation existed between the turbulent structures within the jet and the formation of impact waves after impingement, which may play a role in combustion instability. If a link was detected, these findings could then be used to suggest remedies for combustion instability through boundary layer modification.

Measurements in a straight, circular orifice with L/D=2.5 revealed the presence of a vena contracta at the orifice inlet, as expected. Subsequent measurements were taken at three locations, x/D=0.2, 1.25, and 2.3, first with a free jet at the exit and, at the two upstream locations, with a plate angled at 30° to the jet to simulate impingement for a doublet injector element with $2\theta=60°$. Two phenomena were of interest: changes in the boundary layer and alterations of the turbulence characteristics. Velocity profile comparisons at the two upstream locations revealed no alteration of the boundary layer, and comparisons of axial turbulence intensity profiles and power spectral density analysis of the time marked velocity measurements revealed no change in turbulence characteristics.

Similar measurements were performed in the angled orifice, with similar results. No alteration in the boundary layer thickness or turbulence characteristics was observed. As a result, this possible mechanism for generating the instability characteristics observed in rocket combustors may be eliminated.

Preliminary measurements were also conducted in the free jet, just prior to the point of impingement. Comparison of these results revealed a significant difference between the velocity profiles and the axial turbulence intensity profiles for the two cases, indicating that the downstream impingement does perturb the upstream flow immediately ahead of the point of impingement. In particular, the impingement actually widens the jet and increases the turbulence found in the jet flow field. However, earlier measurements indicate that these disturbances are not propagated upstream to the orifice.

In addition to the liquid jet experiments, analysis of the rocket combustion chamber studies initiated under a previous grant was completed [Santoro, 1997]. The results of that analysis along with a description of the experiments is contained in the attached appendix.

5.0 REFERENCES

Anderson, W. E., Ryan, H. M., Pal, S. and Santoro, R. J., "Fundamental Studies of Impinging Liquid Jets," AIAA 92-0458, 30th Aerospace Sciences Meeting, January 1992.

Anderson, W. E., Ryan, H. M. and Santoro, R. J., "Combustion Instability Mechanisms in Liquid Rocket Engines Using Impinging Jet Injectors," AIAA 95-2357, 31st AIAA/ASME/SAE/ASEE Joint Propulsion Conference, July 1995.

Anderson, W. E., and Santoro, R. J., "The Effects of Drop Size Distribution and Atomization Periodicity on Combustion Response," AIAA Paper No. 96-3027, 32nd AIAA/ASME/SAE/ASEE Joint Propulsion Conference and Exhibit, Lake Buena Vista, FL, July 1-3, 1996.

Durst, F., Jovanovic, J. and Sender, J., "LDA Measurements in the Near-wall Region of a Turbulent Pipe Flow," Journal of Fluid Mechanics, V. 295, March 1995, pp. 305-335.

Heidmann, M. F. and Humphrey, J. C., "Fluctuations in Spray Formed by Two Impinging Jets," Journal of the American Rocket Society, June 1952, pp. 127-131.

Hoehn, F. W., Rupe, J. H. and Sotter, J. G., "Liquid-Phase Mixing of Bipropellant Doublets," JPL Technical Report 32-1546, February 1972.

Ito, J. I., "A General Model Describing Hydraulic Flip in Sharp Edge Orifices," 7th JANNAF Meeting, February 1971, pp. 417-426.

Ruiz, F., "A Few Useful Relations for Cavitating Orifices," ICLASS-91, July 1991, pp. 595-602.

Rupe, J. H., "A Dynamic-Head Probe for Evaluating the Properties of Free Liquid Jets," JPL Progress Report 20-299, May 1956.

Ryan, H. M., Anderson, W. E., Pal, S. and Santoro, R. J., "Atomization Characteristics of Impinging Liquid Jets," Journal of Propulsion and Power, Vol. 11, No. 1, pp. 135-145, 1995.

Santoro, R. J., "High Pressure Combustion Studies Under Combustion Driven Oscillatory Flow Conditions," AFOSR Final Technical Report, Grant F49620-94-1-0235, October 1997.

TSI Incorporated, *System 9100-7 Laser Doppler Velocimeter Instruction Manual*, TSI Incorporated, 1987.

6.0 PUBLICATIONS/THESES

R. J. Santoro, R. Woodward, J. Schmidt, D. Johnson, S. Yeralan, S. Pal, and W. E. Anderson, "Impinging Jet Flow Structure and Its Impact on Combustion Instability," AIAA 98-3536, 34th AIAA/ASME/SAE/ASEE Joint Propulsion Conference, July 1998.

W. E. Anderson, K. L. Miller, H, M. Ryan, S. Pal, and R. J. Santoro, "Effects of Periodic Atomization on Combustion Instability in Liquid-Fueled Propulsion Systems," Journal of Propulsion and Power, Vol. 14, No. 5, Sept.-Oct. 1998.

J. R. Schmidt, "Impinging Jet Dynamics," Master's Paper, The Pennsylvania State University, 1999.

7.0 PARTICIPATING PROFESSIONALS

Prof. Robert J. Santoro, Professor of Mechanical Engineering, Principal Investigator

Dr. William E. Anderson, Research Associate, Mechanical Engineering Department

Dr. Roger Woodward, Research Associate, Mechanical Engineering Department

Dr. Serdar Yeralan, Post-Doc, Mechanical Engineering Department

Dr. Sibtosh Pal, Senior Research Associate, Mechanical Engineering Department

Mr. Dave Johnson, Research Assistant, Mechanical Engineering Department

Mr. John R. Schmidt, Graduate Student, Mechanical Engineering Department (MS, 1999)

Mr. Eric Mouille, Exchange Student from France

Mr. Larry Schaaf, Senior Research Technician, Mechanical Engineering Department

APPENDIX

Effects of Periodic Atomization on Combustion Instability in Liquid-Fueled Propulsion Systems

by

W. E. Anderson, K. L. Miller, H. M. Ryan, S. Pal, R. J. Santoro and J. L. Dressler

Published in

Journal of Propulsion and Power, Vol. 14, No. 5, September-October 1998, pp. 818-825.

JOURNAL OF PROPULSION AND POWER
Vol. 14, No. 5, September–October 1998

Effects of Periodic Atomization on Combustion Instability in Liquid-Fueled Propulsion Systems

W. E. Anderson,* K. L. Miller,† H. M. Ryan,‡ S. Pal,§ and R. J. Santoro¶
Pennsylvania State University, University Park, Pennsylvania 16802
and
J. L. Dressler**
Fluid Jet Associates, Spring Valley, Ohio 45370

A detailed understanding of the mechanism by which combustion instability occurs in liquid rocket engines does not exist. This paper examines the specific role that atomization may play in combustion instability. The effects of mean drop size, drop size distribution, and atomization periodicity are examined explicitly with a combustion response model, whose results indicate that all of these effects are important. It is shown that periodic atomization results in large variations in the magnitude of the pressure response when the atomization frequency is within a factor of 10 of the acoustic oscillation frequency. These results are consistent with an explanation of an empirical stability correlation, whereby the nonuniform and unsteady production of drops is a controlling factor in the growth of combustion instabilities. Experimental results from a subscale rocket combustor that support the importance of periodic atomization are presented. Atomization was electromechanically forced at frequencies from 2000 to 8000 Hz to accentuate the natural tendency for periodic atomization associated with impinging jet injectors. High-amplitude pressure oscillations at frequencies corresponding to the forced atomization frequencies substantiate the importance of periodic atomization. Pressure oscillation amplitudes approaching 10% of mean chamber pressure were measured when the drivers were operating at near optimal conditions. A conceptual model that is consistent with both these results and the empirical correlation is provided.

Nomenclature

a = sound speed
d = diameter
f = frequency or number distribution
h = sheet thickness
m = mass
m' = unsteady vaporization rate
$\dot{m}$ = mass flow rate
p' = unsteady pressure amplitude
R = response factor
S = ρ_{amb}/ρ_j
t = time
U = velocity
v = velocity
We = Weber number
x = axial distance from impingement point
α = spray angle
γ = specific heat capacity ratio, c_p/c_v
θ = impingement half angle
λ = wavelength
ρ = density
σ = surface tension
ϕ = phase angle or angular coordinate on the sheet
ω = radial frequency

Subscripts

amb = ambient
atom = atomization
b = breakup
beat = beat
CL = centerline
coolant = coolant
d = drop
f = fuel
g = gas
inst = instability
j = jet
l = liquid
lig = ligament
o = initial or orifice
oxidizer = oxidizer
trans = transverse
1 = jet 1
2 = jet 2
10 = arithmetic mean
32 = Sauter mean

Introduction

FOR many launch applications the use of liquid (noncr ogenic) fuel is desirable. Liquid fuels, i.e., hydrocarbo (HC), are much denser than hydrogen and easier to handl These attributes are particularly advantageous for the first sta of a multiple-stage, low-cost system, for instance, or f launch-on-demand applications. Usually, liquid oxygen (LO is used in conjunction with liquid HC fuels. A major issue

Received Sept. 2, 1997; revision received March 31, 1998; accepted for publication May 4, 1998.

*Research Associate, Department of Mechanical Engineering; currently Senior Principal Propulsion Engineer, Orbital Sciences Corporation, Chandler, AZ 85248. E-mail: andersonw@orbital-lsg.com. Member AIAA.

†Research Assistant, Department of Mechanical Engineering. E-mail: K1M156@psu.edu.

‡Research Assistant, Department of Mechanical Engineering; currently Development Associate, Praxair, Inc., Tarrytown, NY 10591. E-mail: harry_ryan@praxair.com.

§Senior Research Associate, Department of Mechanical Engineering. E-mail: s9p@email.psu.edu. Member AIAA.

¶Professor, Department of Mechanical Engineering. E-mail: rjs@email.psu.edu. Member AIAA.

**President/Owner. E-mail: dressler@erinet.com.

the development of LOX/HC rocket engines is whether the occurrence of combustion-generated pressure oscillations, which could lead to catastrophic failure, can be avoided.

The initiation and growth of these pressure oscillations, commonly referred to as "combustion instabilities," are primarily determined by the design of the injector. A good injector design provides oscillation-free operation and acceptable thrust efficiency throughout the operating envelope. Historically, LOX/HC rocket engines have had thrust efficiencies of 3–5% less than their hydrogen-fueled counterparts.[1] This is not because design strategies for efficient combustors are unknown, but rather because the design strategies that lead to very efficient combustion also tend to promote the occurrence of high-frequency combustion instability in LOX/HC rocket engines.

Instabilities can be classified according to whether they occur as bulk mode oscillations or in resonance with the chamber's acoustic modes, as well as by the mechanisms by which they are initiated and amplified.[2,3] Pressure oscillations that are due to fluctuations in the propellant flow rate are referred to as injection-coupled instabilities. Injection-coupled instabilities are amplified when the flow rate oscillations become coupled with either bulk- or acoustic-mode chamber pressure oscillations. Eliminating injection-coupled instabilities (chug instabilities) is accomplished by increasing the injection pressure drop (by reducing the injection flow area, or by increasing the propellant flow rate). Acoustic mode instabilities, which occur at a higher frequency than chug instabilities, can also be because of injection coupling. Longitudinal-mode instabilities are often injection coupled and are acoustic in nature with a pressure antinode at the injector face. Injection-coupled instabilities are well modeled with conventional time lag models and are relatively easy to avoid or eliminate.

More problematic than the injection-coupled instabilities are the instabilities that are intrinsically coupled to the combustion processes. These intrinsic instabilities typically occur with liquid propellants when the energy release density in the combustor is increased; as the energy release density increases, higher modes of combustion instability occur. To eliminate these instabilities, the injection pressure drop is reduced or the injector element orifice size is enlarged, both of which tend to decrease energy release density and combustion efficiency in a fixed volume combustor. This purposeful decrement of performance to achieve combustion stability is the reason that LOX/HC rocket engines such as the H-1 and F-1 have lower combustion efficiencies than do hydrogen-fueled rocket engines.

To develop effective design strategies for the elimination or control of combustion instabilities, it is necessary to define the physical mechanisms that lead to the growth of these instabilities. Most of the work to date on combustion instability mechanisms has been based on the premise that intrinsic instabilities are controlled by vaporization. This premise is based explicitly on the proposition that vaporization is the rate-limiting step in spray combustion. The role of atomization has been dismissed largely on the basis that atomization occurs so rapidly that it could not be rate controlling.

Previous work conducted in our laboratory emphasized measurements of a cold-flow spray formed by impinging jet injectors, which are commonly used with liquid propellants.[4] The measurements included atomization frequency and drop size distribution. The experimental results were compared with an empirical stability correlation for the highest sustainable frequency of combustion instability in rocket engines that use impinging jet injectors.[5,6] It was found that atomization is a periodic phenomenon that occurs on a time scale similar to typical combustion instabilities. Furthermore, the atomization frequency and the highest sustainable frequency of combustion instability indicated by the empirical stability correlation increase linearly with the ratio of injection velocity-to-orifice diameter (U_j/d_o). The measurements also indicated that the average drop size and the polydispersity of the drop size distribution decreased with increasing U_j/d_o.

Although the impinging jet measurements indicated a clear periodic nature to the atomization process, there was a definite unsteady character evident as well.[5,6] Even though an average frequency was determined that was three to four times higher than the highest sustainable frequency indicated by the empirical correlation, some variation in the atomization frequency occurred. It is argued that under such conditions, interactions with the acoustic field of the combustion chamber will determine which frequency, if any, will intrinsically couple to the combustion process.

To investigate this topic further, the present work considers both theoretical and experimental approaches to gain further insights. In the theoretical approach a model is developed that allows the combustion response calculation that is a result of the vaporization process when periodic atomization is included. In the experimental approach a novel electromechanical modulation technique is used to affect the atomization frequency. This modulation results in a sharper periodic atomization frequency compared with the previously studied unsteady case. Although the modulation is applied to the liquid flow in the injector, it is argued that this approach preferentially establishes a narrow frequency range for the periodic atomization from among the broader atomization frequencies occurring naturally. Thus, this approach still allows the examination of intrinsic combustion instability behavior.

Analysis

Model Description

The combustion response methodology is a standard approach for analyzing combustion stability.[7] In this analysis the changes in the combustion rate because of ambient oscillations are calculated and integrated to determine the amount of the heat release that occurs in phase with the pressure oscillation. A large positive value of combustion response at a given frequency indicates that a potential for a coupling between acoustic oscillations and heat release exists if the frequency corresponds to an acoustic mode of the chamber; combustion instability may then occur.

Usually the combustion response is approximated by the vaporization response. The in-phase response factor R is defined as

$$R = \int_0^{t_d} m'p'\,dt \Big/ \int_0^{t_d} (p')^2\,dt \tag{1}$$

where t_d is the drop lifetime. In the present implementation of the combustion response analysis, an open-loop response is calculated. Theoretically, a value of R of at least $(\gamma + 1)/2\gamma \sim 0.9$ is required to drive a longitudinal instability for the case of concentrated combustion at the pressure antinode of a closed chamber, where γ is the specific heat capacity ratio of the gas. In the present analysis, the Priem–Heidmann model is used to calculate the vaporization rate.[8]

A standing transverse acoustic wave in a two-dimensional chamber was considered in the analysis, thus, the pressure oscillates in a sinusoidal fashion:

$$p' \propto \cos(\omega t) \tag{2}$$

The pressure oscillations are accompanied by out-of-phase transverse velocity oscillations:

$$v_{\text{trans}} \propto \sin(\omega t) \tag{3}$$

The maximum amplitude of the pressure oscillation was set at 0.1 times the mean chamber pressure. The order of the amplitude of the transverse velocity oscillation associated with a

pressure oscillation of p' is $(a/\gamma)p'$. This condition corresponds to a location in the chamber that is intermediate between a pressure antinode and a pressure node, where both oscillations in velocity and pressure are present.

The combustion response analysis is a straightforward and mechanistic means of predicting combustion stability characteristics. Accurate accounting of the combustion processes is the main difficulty. Of all the component combustion processes, atomization is possibly the most difficult to model accurately. Consequently, most applications of the combustion response analysis greatly simplify the atomization process. Typically, an array of drops, all of the same size, is used to represent the actual distribution of drop sizes and velocities. The representative drop is injected continuously over one cycle of the pressure oscillation. These injection rates range from about 16 to 36 times per cycle.[7,9] However, the effects of periodic atomization and drop size distribution should be included in the analysis.

A phenomenological model of atomization for impinging jet injectors was developed earlier and will only be briefly reviewed here.[10] The phenomenological model has three main steps: 1) Fan formation and the appearance of impact waves, 2) fragmentation of the fan into ligaments and other large structures, and 3) the disintegration of ligaments and large drops into small drops that represent the quasiequilibrium end state of atomization. Impact waves are observed to form directly following the impingement of the liquid jets and have a characteristic length on the order of the jet diameter. These waves are convected down the sheet at a speed equal to the liquid jet velocity. Thus, the highest atomization frequency predicted by this model corresponds to $U/\lambda \sim U_j/d_o$, and is shown in Fig. 1 expressed in terms of a Strouhal number as $fd_o/U_j \sim 1$. This highest atomization frequency is compared to results from an empirical stability correlation of the highest sustainable frequency of combustion instability (referred to as the high-frequency cutoff) that can be driven by a given impinging jet injector design. It is seen that the highest sustainable frequency of combustion instability is about 10 times less than the highest atomization frequency. This will be shown to have a major impact on the magnitude of the combustion response. The fact that the atomization frequency and the highest sustainable frequency of combustion instability are both described by the same nondimensional parameter suggests a strong coupling mechanism between periodic atomization and combustion instability.

A model was developed that accounted for the processes described in the preceding text.[10] The average size of the ligaments, d_{lig}, that are shed off the leading edge of the liquid fan can be determined from the wavelength of the impact waves λ and the thickness h_b of the sheet at the point where the sheet breaks up as discussed in Ref. 10, i.e.,

$$d_{lig} = \sqrt{4\lambda h_b/\pi} \tag{4}$$

where h_b can be determined from[11]

$$h_b = \frac{d_o^2 \sin^3\theta}{4x_b(1 - \cos\phi\cos\theta)^2} = \frac{d_o^2}{4x_b} f(\theta) \tag{5}$$

A correlation for the dependence of λ on x_b from data obtained in cold flow studies[10] yields

$$\lambda/d_o = 0.687 + 0.1019(x_b/d_o) \tag{6}$$

Furthermore, because x_b also changes with ambient pressure, a correlation was developed for x_b as a function of jet conditions and ambient pressure based on the product of the square of the density ratio $s = \rho_{amb}/\rho_j$, and the jet Weber number We_j[10]

$$x_b/d_o = 13.56(We_j s^2)^{-0.102} \tag{7}$$

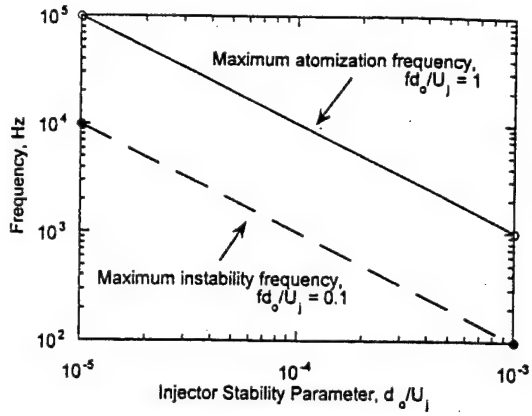

Fig. 1 Comparison of atomization frequencies associated with impinging jet injectors and combustion instability frequencies.

Equations (4–7) can be combined to yield an equation for the average diameter of a ligament shed off the liquid fan. Because most drop size measurements have been taken at the centerline of the fan, i.e., $\phi = 0$, the centerline ligament diameter was calculated to be

$$\left.\frac{d_{lig}}{d_o}\right|_{CL} \approx 0.22\sqrt{\left[\frac{f(\theta)}{\pi}\right][(We_j s^2)^{0.102} + 2]} \tag{8}$$

The disintegration of the ligaments into drops was also treated through a correlation for d_{32}/d_{lig} that relies on Eq. (8) and correlations that exist for drop size as a function of impinging jet geometry and flow conditions[12] (also see Ref. 10), and yields

$$\frac{d_{32}}{d_{lig}} = 1.008(We_{g,lig})^{-0.136} \tag{9}$$

where $We_{g,lig}$ is the ligament Weber number based on the gas density. Finally, using Eqs. (6) and (7) to determine the wavelength of the impact waves λ, and the fact that the impact waves travel along the sheet at a velocity U_j, the atomization frequency predicted by the model can be calculated (Table 1).

The combustion response analysis used here considers heptane drops burning in an oxygen environment. The measured size distribution for a water spray formed by impinging jets was converted to a heptane spray size distribution by accounting for the property differences of ambient gas density, liquid density, and surface tension by using the following correlation[12]:

$$d_d \propto \sigma^{0.16}(\rho_l/\rho_g)^{0.1} \tag{10}$$

The ambient pressure chosen for the study was 1.72 MPa (250 psia), which is approximately the nominal design pressure of the combusting flow tests that proceeded in parallel. The molecular weight of the products of heptane–oxygen combustion is 30 kg/kmole and the ambient gas temperature was chosen to be 3500 K. The resultant heptane drop size distribution used in the combustion response analysis is shown in Fig. 2. Note that the distribution was based on the measured water spray and adjusted for property differences. Table 1 provides a summary of the cases considered in the combustion response analysis at the conditions employed in the analysis, including the stability parameter d_o/U_j, the high-frequency cutoff based on the empirical stability correlation,[5] and the atomization frequency as calculated from an atomization model developed earlier.

Results

The vaporization rates of the drops under nonoscillatory conditions are shown in Fig. 3. The rates are normalized by

Table 1 Study cases used in response analysis of heptane/oxygen combustion

Case number	d_o/U_j, seconds $\times 10^5$	High-frequency cutoff, Hz	Atomization frequency, Hz	d_{10}, μm	d_{32}, μm
1	2.59	3861	15,914	110	372
2	3.43	2915	11,529	133	389
3	4.10	2439	9,391	154	455
4	5.12	1953	7,272	182	472
5	9.98	1002	3,365	383	576

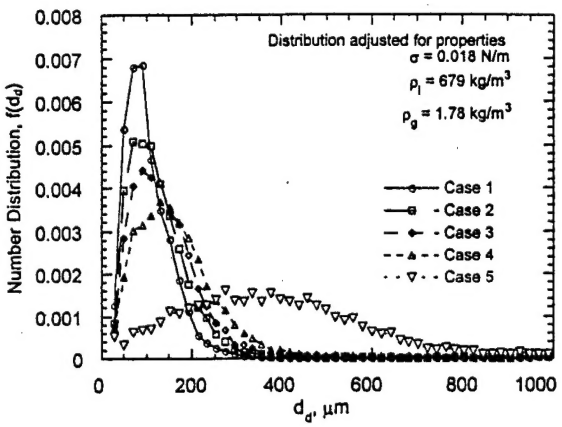

Fig. 2 Number distribution of heptane drops used in the combustion response analysis.

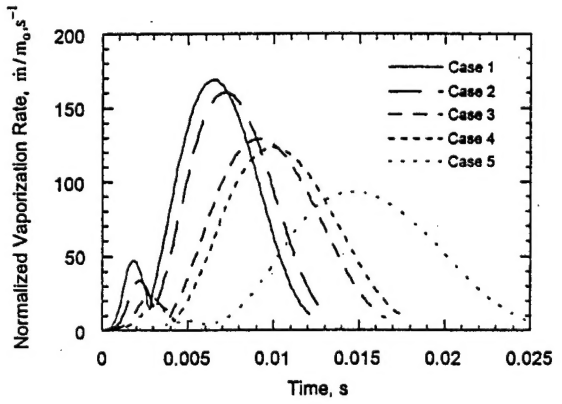

Fig. 3 Normalized vaporization rate of a heptane drop.

the initial mass of the drop m_o. The smallest mean-size drop (case 1, $d_{32} \sim 372$ μm) vaporizes within 12 ms, whereas the largest drop (case 5, $d_{32} \sim 576$ μm) takes about 25 ms to vaporize. The drop undergoes a regime where the difference between its velocity and the ambient gas velocity is a minimum, and this regime is indicated most clearly by the local minima in the vaporization rate. This regime, which occurs at about 3 ms for the smallest drop (case 1) and at about 6 ms for the largest drop (case 5), is the regime that Priem and Guentert regarded as being most unstable because here the drops are most susceptible to transverse velocity oscillations associated with the unsteady flowfield.[13]

Three different approaches were used to calculate vaporization response. The first approach is conventional and uses a mean drop size (d_{32}) to represent the spray. The continuous atomization approximation is used. For the second approach, the distribution of heptane drops shown in Fig. 2 is injected continuously over the period of oscillation. For both approaches using continuous atomization, the time interval between each injection was 1/16 of the period of oscillation, which is the value recommended in the ROCCID code.[14] Each of these approaches also uses the experimental data from Table 1 and Fig. 2 as input to the model. Because the drop size is dependent on the atomization frequency, it is difficult to uncouple the effects of drop size and atomization frequency. Thus, the third approach is a parametric study of the effects of periodic atomization on the combustion response of a single drop of a given size when the atomization frequency is on the same order as the pressure oscillation frequency.

Mean Drop Size, Continuous Atomization

Figure 4 shows the vaporization response of continuously atomized drops with a diameter equal to the Sauter mean diameter (d_{32}) of the distribution. The frequency at which the peak response occurs is inversely proportional to drop size, and ranges from about 60 Hz for the 576-μm drop to about 110 Hz for the 372-μm drop. The magnitude of the peak response is essentially independent of drop mean diameter and is about 0.75. These results are consistent with many of the response calculations reported previously that indicated response magnitudes too low to drive an instability.[7,9,15] The frequencies corresponding to the predicted peak response magnitude, which are dependent on the drop mean diameter, are much lower than the high-frequency cutoff values indicated in Table 1.

Size Distribution, Continuous Atomization

Figure 5 shows the vaporization response for the continuously atomized distribution of drops. The peak vaporization responses are attenuated by about 50% as compared to those of the continuously atomized mean drop sizes. For case 1, the case with the smallest mean drop size and the least disperse distribution, the peak response is 0.32 and occurs at a frequency of about 900 Hz. The peak response magnitude for case 5, having the largest mean drop size and the most disperse distribution, is 0.31 at a frequency of about 100 Hz. The magnitude of the response is insufficient to drive an instability for either the mean drop size-based or the distribution-based method. The use of the drop size distribution rather than the mean drop size also has an effect on the width of the response.

A comparison of the peak response frequencies predicted by the combustion response model with the high-frequency cutoff predicted by the empirical stability correlation (see Table 1) reveals that either application of the response analysis tends to underpredict the most amplified frequency. It is important to note that the empirical stability correlation does not necessarily represent the frequency with the highest growth rate; rather, it is the highest frequency of instability that has been observed in practical combustors.

Effects of Unsteady Atomization

Calculations were also done where the atomization frequency listed in Table 1 was used in conjunction with the drop size distribution of Fig. 2. This is a more realistic case than was considered in either of the prior two approaches. The calculated combustion response magnitudes for this periodic atomization case were significantly larger than for the case of drop size distribution with continuous atomization. The combustion response magnitude was also dependent on the phase angle ϕ between the pressure oscillation and the onset of periodic atomization. A parametric study of the effects of periodic atomization was performed because the exact relationship between atomization and the pressure oscillations can only be assumed. Drops with diameters ranging from 10 to 100 μm and atomization frequencies ranging from 5 to 15 kHz were

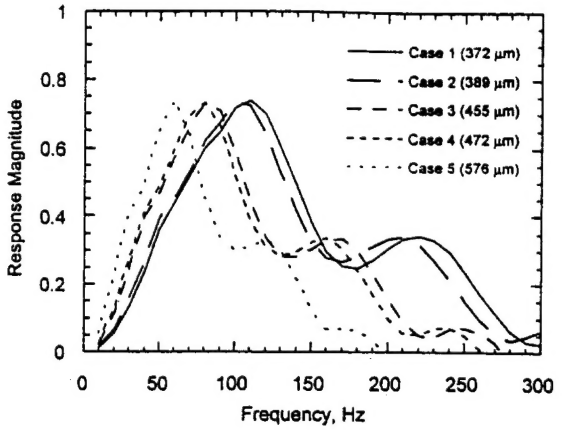

Fig. 4 Vaporization response magnitude for continuously atomized, mean-sized heptane drops as a function of ambient pressure oscillation frequency.

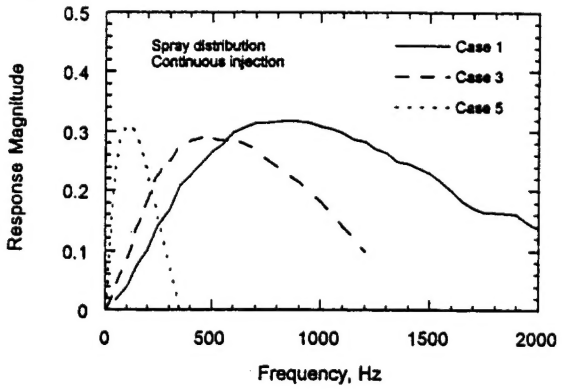

Fig. 5 Vaporization response magnitude for continuously atomized heptane drops with a drop size distribution shown in Fig. 2 as a function of ambient pressure oscillation frequency.

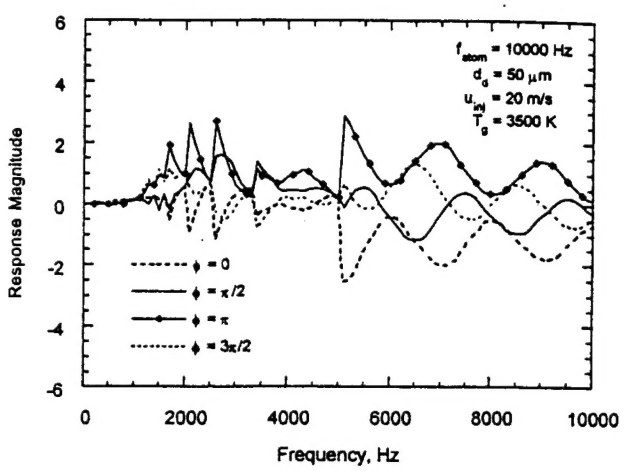

Fig. 6 Vaporization response magnitude as a function of ambient pressure oscillation frequency and phase angle ϕ.

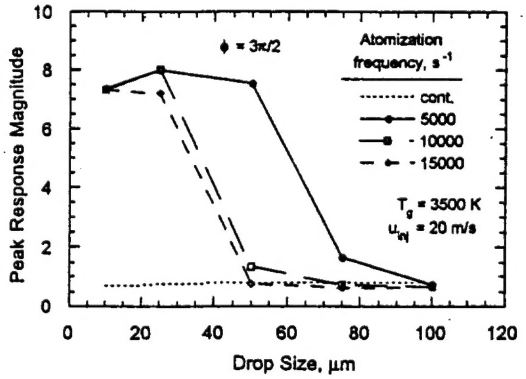

Fig. 7 Peak response magnitude as a function of drop size and atomization frequency for constant phase angle ϕ.

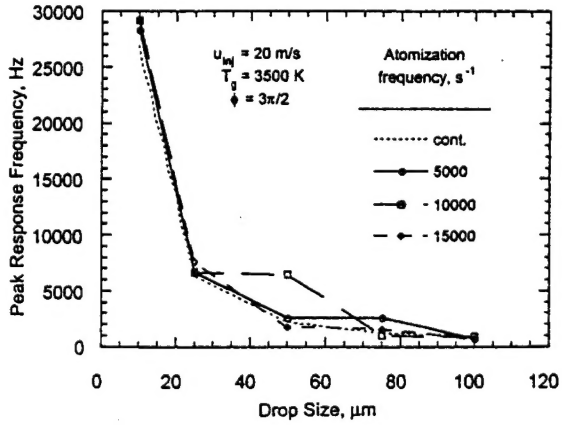

Fig. 8 Frequency at peak response magnitude as a function of drop size and atomization frequency for constant phase angle.

varied independently to evaluate their effects on the response function.

Representative results of the calculated response magnitude as a function of ambient pressure oscillation frequency and phase angle are shown in Fig. 6 for the 50-μm drop size case. For this case, the atomization frequency was 10 kHz. For all cases with periodic atomization, the peak response factor was significantly greater than 1, even approaching a value of eight for the 10-μm drop size case (not shown). Calculations indicated that the peak response magnitude decreased with increasing drop size. With increasing drop size, the peak response frequency was also reduced. These results indicate the potentially dominating effects of periodic atomization on response magnitude and, thus, the growth of the instability.

The effects of periodic atomization and drop size on the calculated peak response magnitude are shown in Fig. 7. The phase angle ϕ was held constant for these calculations. A comparison with the peak response magnitude calculated using continuous atomization reveals that order-of-magnitude increases in response magnitude are possible with periodic atomization. Large response magnitudes are calculated for small drops (10 and 25 μm) at all values of atomization frequency. For the larger drop sizes, response magnitude generally increases with decreasing atomization frequency, although peak response values remain above the continuous atomization value. The effects of periodic atomization extend further into the large drop size region as the atomization frequency is decreased.

The effects of periodic atomization on the peak response frequency are considerably less significant, as shown in Fig. 8. Again, the calculated values of peak response frequency corresponding to continuous atomization are shown for comparison. Generally, the peak response frequency calculated with periodic atomization is consistent with the calculated peak response frequency for continuous atomization, although there were some peculiar cases requiring further study where significant differences occurred.

Experiments

Experiments were conducted to determine the conditions under which periodic atomization could cause longitudinal-mode

combustion instabilities in a model rocket combustor using gaseous oxygen and liquid ethanol as propellants. The gaseous oxygen entered the combustor through a cavity at the injector plane. The experimental setup was composed of the model rocket combustor, an impinging jet injector, piezoelectric drivers, high-frequency pressure transducers, and associated flow delivery and data acquisition equipment. Details of the experimental setup are provided elsewhere.[16]

The chamber used in the combustion modulation tests is 10 in. long, and has a 50.4 × 50.4-mm (2 × 2-in.) internal cross section. The frequency of the fundamental longitudinal mode of the chamber was calculated to be 2200 Hz, based on a 250-mm (10-in.) long combustor and gas properties calculated from a one-dimensional chemical equilibrium program. The combustor was instrumented with high-frequency pressure transducers at approximately 13.0 mm (0.5 in.) downstream of the injection plane and at approximately 38.1 mm (1.5 in.) upstream of the start of the nozzle convergence. This allowed dynamic pressure measurements near the two pressure antinodes. The pressure transducers were calibrated in situ. The linearity of each transducer was 0.363 μV/Pa (2.5 mV/psi). The signal from the high-frequency pressure transducers was sent to a data acquisition system at a rate of 50 kHz, and stored on a personal computer for later analysis. The raw high-frequency pressure signal was also sent to a fast Fourier transform spectrum analyzer for real-time analysis of the power spectral density (PSD) of the chamber pressure oscillations. The PSD was monitored during the tests to evaluate the performance of the electromechanical drivers and to guide the driver configuration.

An impinging jet injector was used, having an orifice diameter of 1.0 mm (0.040 in.) and an included impingement angle of 60 deg. The active injector element was based on technology developed earlier,[17] with the basic design of the electromechanically driven injector assembly shown in Fig. 9. The assembly, 0.152 m (6 in.) in length, is comprised of piezoelectric drivers and a nozzle holder. The driver consists of the piezoelectric transducers, a center bolt, and a piston. Fluid enters the top of the assembly and travels through the hollow center bolt to a fluid manifold, which is formed by the piston surface and an orifice plate. A voltage applied to the transducers causes the piezoelectric material to expand, and the piston is pushed toward the fixed orifice plate. As the voltage to the piezoelectric goes to zero, the center bolt provides the restoring force that draws the piston back to its original position. The voltage signals are provided to the injector system by a function generator, a power amplifier, and matching transformers.[17] The function generator can supply any required signal form, including noise.

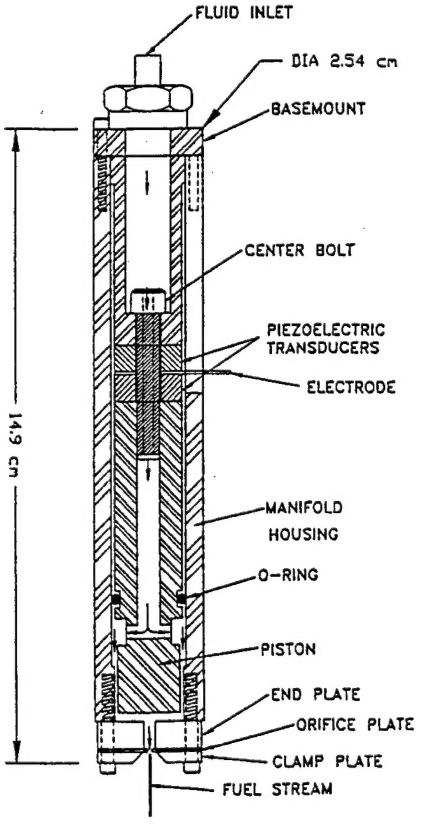

Fig. 9 Electromechanically driven injector assembly.

The electromechanical drivers were incorporated into the injector such that each of the two impinging jets could be driven independently. This allowed different perturbation frequencies to be imposed on the jets, as well as variations in the phase angle between the signal to each jet. Figure 10 is an image of a water spray formed by the driven impinging jet injectors at atmospheric conditions. For the case shown in Fig. 10, the jet velocity is 5.2 m/s, the included impingement angle is 60 deg, and the orifice diameter is 1.0 mm (0.04 in.). The driving force placed on each jet enhances the naturally occurring periodic atomization associated with the impinging jets.

The signals to the electromechanical drivers were established prior to starting the hot-fire test sequence, and left on throughout the test. The drivers were run either at the same frequency, or at different frequencies to produce a beat frequency. Drivers run at the same frequency were run either in-phase or out-of-phase with each other. In-phase driving yielded the highest pressure oscillation amplitude in the combustion tests.

The flexibility of the experimental configuration allowed the test conditions to be changed rapidly. Over 50 variations of driving conditions/flow conditions were tested. The lowest driving frequency tested was 1800 Hz, and the highest driving frequency tested was 8000 Hz. The most effective driving was achieved at the highest flow rate. Chamber pressure and the oxidizer to fuel ratio (O/F) were held relatively constant for all tests, at about 1.45 MPa (210 psia) and 1.7, respectively. The chamber pressure was held constant for different flow rates by changing the nozzle throat diameter.

The frequency of the first longitudinal frequency was calculated to be about 2200 Hz for all conditions. Later it was measured to be about 1850 Hz. The stability parameter in Table 2 is the value of the dimensionless parameter fd_o/U_j, where f is the pressure oscillation frequency (the first longitudinal frequency in this case, 2200 Hz), d_o is the orifice diameter (1 mm), and U_j is the fuel injection velocity (see Table 2). The empirical stability correlation indicated that the stability parameter must be less than about 0.1 for instability to occur. Thus, cases C, D, and E would be capable of driving an instability at the frequency of the first longitudinal mode. Case D also satisfies the condition to drive a second longitudinal mode (f = 4400 Hz, $fd_o/U_j \sim 0.1$). Case E could nearly drive a third longitudinal mode (f = 6600 Hz, $fd_o/U_j \sim 0.12$) as well

Fig. 10 Spray formed by electromechanically driven impinging injector. Jets are perturbed out-of-phase at 2500 Hz.

Table 2 Combustion modulation test conditions

Operating Parameters	Case A	Case B	Case C	Case D	Case E
$\dot{m}_{fuel}$, kg/s	0.019	0.025	0.031	0.056	0.070
$\dot{m}_{oxidizer}$, kg/s	0.032	0.043	0.053	0.095	0.119
$\dot{m}_{coolant}$, kg/s	0.0068	0.0068	0.0068	0.016	0.016
O/F	1.70	1.71	1.71	1.69	1.69
Pc, MPa	1.43	1.62	1.44	1.57	1.52
D_{throat}, mm	8.76	9.55	11.3	14.6	16.6
f, Hz	2200	2212	2208	2213	2212
U_j, m/s	15	20	25	44	55
fd_o/U_j	0.147	0.110	0.089	0.051	0.0378

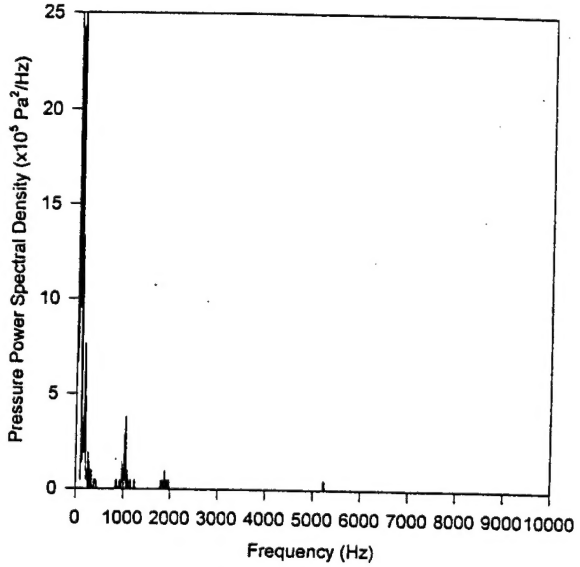

Fig. 11 Pressure PSD. Peaks show first (1850 Hz), second (3700 Hz), and third (5200 Hz) longitudinal modes.

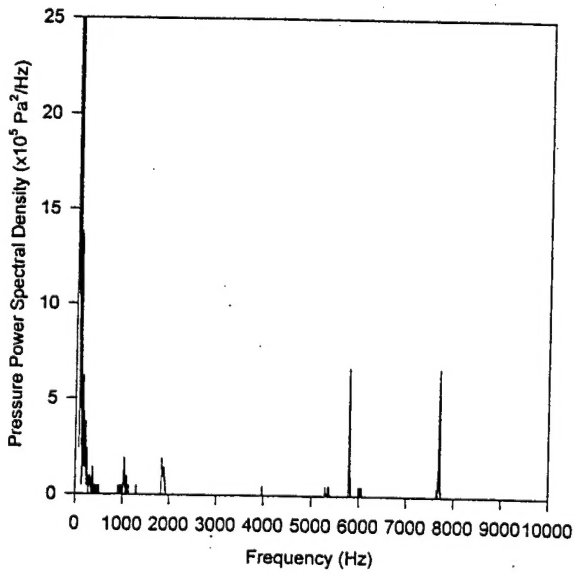

Fig. 12 Pressure PSD. Case E in which jets are driven at 7700 and 5800 Hz to produce a beat frequency of 1900 Hz.

the first and second longitudinal modes, and this was shown to be the case in the experiments.

Results

A plot of the PSD for case E with no signal to the electromechanical drivers is shown in Fig. 11. Significant electronic noise was measured below 600 Hz. Small peaks at about 1850, 3700, and 5200 Hz were measured, corresponding to the first, second, and third longitudinal modes, respectively, and indicating a highly damped chamber. A peak is also observed near 1000 Hz, whose source is not presently known. This peak is observed in all of the results, but is significantly smaller than the larger pressure oscillations observed under conditions for which driving is applied to the jets (see Figs. 12 and 13). It was found that driving the jets near the first longitudinal frequency did not produce significant levels of chamber pressure oscillations. This was primarily because of the low power output of the piezoelectric drivers at frequencies below about 4000 Hz. However, it was possible to drive significant first longitudinal pressure oscillations by causing a beat atomization frequency near 1900 Hz, as shown in Fig. 12. In this case, a 7700-Hz signal was sent to one of the jets, and a 5800-Hz signal was sent to the other jet to produce the beat frequency of 1900 Hz.

The highest levels of pressure oscillations were achieved with high flow rates and driving frequencies of about 5500 Hz, with an in-phase signal provided to the jets as shown in Fig. 13. In this case, both the first and the third longitudinal frequencies were driven. Chamber pressure time traces shown in

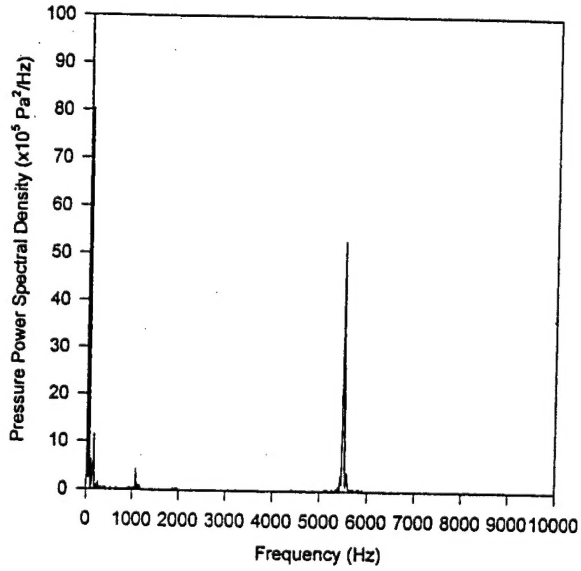

Fig. 13 Pressure PSD. Case E in which jets are driven at 5500 Hz.

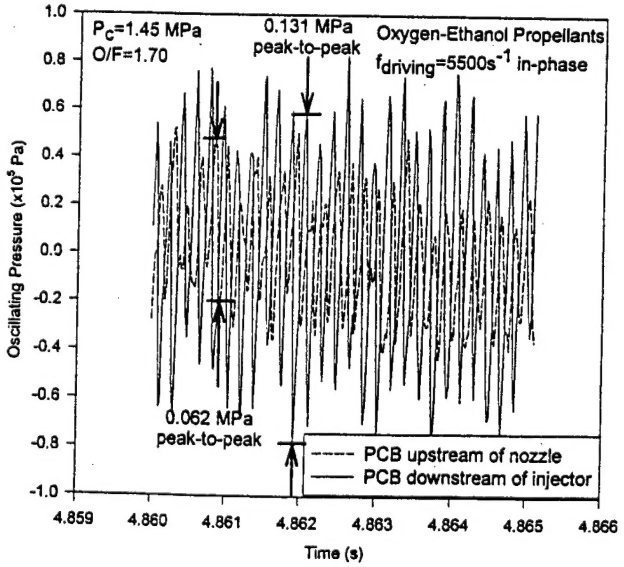

Fig. 14 Time traces of chamber pressure corresponding to the PSD of Fig. 14. The sampling rate is 50 kHz.